SEARCHING FOR SM-LIKE HEAVY NEW QUARKS AT THE LHC

by

Merve Şahinsoy

B.S., Physics, Bilkent University, 2011

Submitted to the Institute for Graduate Studies in
Science and Engineering in partial fulfillment of
the requirements for the degree of
Master of Science

Graduate Program in Physics

Boğaziçi University

2015

ACKNOWLEDGEMENTS

This study has greatly benefited from the academic guidance of my supervisors. First of all, I would like to thank my thesis advisor V. Erkcan Özcan. If he did not decide to come back to Turkey, this study wouldn't even start and exist. I am really grateful for his support and trust. His guidance during my master degree has been really valuable for me. I would like to express my gratitudes to my co-supervisors Gökhan Ünel and Tülay Çuhadar Donszelmann. They have spent their time to make this study possible. Also, special thanks to Gökhan Ünel, since he played a crucial role in my educational career and initiated this study.

I would like to thank my teammate İsmet Sıral for his contributions to my thesis and his valuable friendship; Serhat Işтın and Mehmet Şahin for their helps. I would like to present my special thanks to Metin Arık and Serkant Ali Çetin for their support.

I would also like to thank all my friends in Engin Arık High Energy Physics Laboratory and my friends Özlem Salehi, Bahar Özkan and especially Aybüke Yedidag. Finally, I would like to thank special people in my life for their endless support and love. They have suffered with me during this thesis and have always believed in me; Sevgi and Rıfat Şahinsoy, Asli Sim and Semih Karacasu.

Writing this thesis was not only a scientific study but also an adventurous journey for me. There have been tough moments during this path, but in the end, it worths for all the effort. I am grateful to ATLAS Collaboration to make this study possible and I acknowledge the support from TAEK during my stay at CERN.

ABSTRACT

SEARCHING FOR SM-LIKE HEAVY NEW QUARKS AT THE LHC

This thesis describes the search performed with the ATLAS detector for heavy quarks (denoted as Q) in the $Q\bar{Q} \rightarrow WqWq$ channel where one W boson decays leptonically and the other hadronically. Final state of this processes is four jets, one lepton and missing transverse energy. The analysis is based on an integrated luminosity of 20 fb^{-1} data collected during the 2012 from proton-proton collisions at a centre-of-mass energy of 8 TeV. No significant excess of events above the Standard Model expectation is observed and lower limit on the Q quark mass has been set at 519 GeV for electron channel and 475 GeV for muon channel with 95% confidence level.

ÖZET

ATLAS DENEYİNDE STANDART MODEL BENZERİ YENİ AĞIR KUARKLARIN ARAŞTIRILMASI

Bu tezde ATLAS detektöründe $Q\bar{Q} \rightarrow WqWq$ süreciyle bozunan ağır kuarkların (Q'yla gösterilmektedir) yarıleptonik olarak bozunduğu son durumlar incelenmektedir. Sürecin sonunda dört jet, bir lepton ve kayıp dik enerji ortaya çıkmaktadır. Analiz edilen veri 20 fb^{-1} entegre ışınlıktadır ve 2012 yılında Büyük Hadron Çarpıştırıcısı'nda (BHÇ) 8 TeV kütle merkezi enerjisiyle çarpıştırılan proton proton demetlerinden elde edilmiştir. Standart Model'in beklentilerinden herhangi bir sapma gözlenmemiştir ve Q kuarkının kutlesi elektron kanalında 519, muon kanalında 568 GeV'e kadar 95% güvenilirlik düzeyinde dışarlanmıştır.

TABLE OF CONTENTS

ACKNOWLEDGEMENTS . . . iii
ABSTRACT . . . iv
ÖZET . . . v
LIST OF FIGURES . . . ix
LIST OF TABLES . . . xiii
LIST OF SYMBOLS . . . xiv
LIST OF ACRONYMS/ABBREVIATIONS . . . xvi
1. INTRODUCTION . . . 1
2. THEORETICAL MOTIVATION . . . 2
2.1. Standard Model . . . 2
2.1.1. Fundamental Particles . . . 2
2.2. Fundamental Forces . . . 3
2.3. Limitations of Standard Model . . . 4
2.3.1. CP Violation . . . 4
2.3.2. Hierarchy Problem . . . 5
2.4. Heavy Quark Searches Beyond the Standard Model . . . 5
3. THE ATLAS EXPERIMENT . . . 8
3.1. LHC . . . 8
3.2. THE ATLAS DETECTOR . . . 9
3.2.1. Coordinates and Nomenclatures . . . 9
3.2.2. Inner Detector and Tracking . . . 10
3.2.2.1. Pixel Detector . . . 11
3.2.2.2. Semiconductor Tracker . . . 12
3.2.2.3. Transition Radiation Tracker . . . 12
3.2.3. Calorimeters . . . 13
3.2.3.1. Electromagnetic Calorimeter . . . 13
3.2.3.2. Hadronic Calorimeter . . . 14
3.2.4. Muon Chambers . . . 15
3.2.5. Trigger and data acquisition . . . 16

4. PHYSICS OBJECTS 18
4.1. Electrons 18
4.1.0.1. Loose Electrons 19
4.1.0.2. Tight Electrons 20
4.2. Muons 20
4.2.0.3. Loose Muons 21
4.2.0.4. Tight Muons 21
4.3. Jets 21
4.4. Missing Transverse Energy 22
5. DATA, BACKGROUND AND SIGNAL SAMPLES 24
5.1. Data 24
5.2. Signal Samples 25
5.3. Backgrounds 25
5.3.1. W+jets 26
5.3.2. $t\bar{t}$ Background 27
5.3.3. Single Top 27
5.3.4. Dibosons 27
5.3.5. Z+jets 28
5.4. Data Driven Corrections and Contributions for Background 28
5.4.1. W+jets Charge Asymmetry Normalization 28
5.4.2. W+jets P_T Momentum Reweighting 29
5.4.3. Fake Contribution 29
6. SEARCHING FOR THE NEW PARTICLE 31
6.1. Event Preselection 31
6.1.1. Data Quality Cuts 31
6.1.2. Object and Event Quality Cuts 33
6.1.3. Trigger Requirement 33
6.1.4. Physics Objects Requirements and Kinematic Selection Criteria 34
6.1.5. Control Regions 35
6.2. Mass Reconstruction 35
6.2.1. Momentum Estimation for Neutrino 36

6.2.2. Jet Association 36
6.3. Loose Analysis Results 38
7. SYSTEMATIC UNCERTAINTIES 43
7.1. Luminosity 43
7.2. Physic Objects Uncertainties 44
7.2.1. Jet Energy Scale 44
7.2.2. Jet Energy Resolution 44
7.2.3. Jet Reconstruction Efficiency 45
7.2.4. Muon Momentum Scale and Resolution 45
7.2.5. Muon top-Id efficiency SF 45
7.2.6. Electron Energy Scale and Resolution 46
7.2.7. Electron Reconstruction, ID efficiency and Isolation Factors . . 46
7.3. Systematic Uncertainty for W+jets Background 47
8. FINAL EVENT SELECTION AND LIMIT SETTING 50
8.1. Tight Cuts 50
8.2. Limit Setting 53
8.3. Final Selection with Light quarks:B-veto 56
9. CONCLUSIONS 59
APPENDIX A: PLOTS FOR FINAL SELECTIONS 60
APPENDIX B: CONTROL REGIONS 64
B.1. Control Region with 3 jets 64
B.2. Control Region with 2 jets 65
B.3. Control Region only with 1 jet 66
REFERENCES 67

LIST OF FIGURES

Figure 2.1. Fundamental particles [1]. 3

Figure 2.2. Possible tree-level SM-like production channels of heavy quarks. . 6

Figure 2.3. Theoretical cross sections at NNLO for $Q\bar{Q}$ production in pp collisions at two center-of-mass energies, $\sqrt{s} = 7$ TeV and $\sqrt{s} = 8$ TeV, computed by HATHOR [3]. 6

Figure 3.1. Atlas Detector [4]. 10

Figure 3.2. Inner Detector [4]. 11

Figure 3.3. ATLAS Calorimeters [4]. 14

Figure 3.4. Schematic overview of the Trigger and DAQ system [7]. 17

Figure 5.1. Feynman diagram of the semileptonic decay channel of the pair produced heavy quarks. 24

Figure 6.1. Reconstructed hadronic W mass in 500 GeV signal sample. 37

Figure 6.2. Mass difference of the reconstructed $Q\bar{Q}$ in 500 GeV signal sample. 38

Figure 6.3. P_T and η of electrons, P_T of jets, E_T^{miss} distribution in electron channel. 39

Figure 6.4. ϕ distributions of the objects, η distribution of the jets in electron channel. 39

Figure 6.5. P_T and η of muons, P_T of jets, E_T^{miss} distribution in muon channel. 40

Figure 6.6. ϕ distributions of the objects, η distribution of the jets in muon channel. 40

Figure 7.1. The effect of the ± 1 σ variations of MS muon momentum smearing on muon P_T distribution of 600 GeV signal sample. 46

Figure 7.2. The effect of the $\pm 1\sigma$ variations of electron energy smearing on electron P_T distribution of 600 GeV signal sample. 47

Figure 8.1. Difference between $M_{Q_{lep}}$ and $M_{Q_{had}}$ after preselection in muon channel. 51

Figure 8.2. Top plots show the mass difference between reconstructed new quarks, left bottom plot is the cosine of the angle between two jets coming from the Q quarks, right bottom plot is cosine of the angle between two jets forming the W_{had} after preselection in electron channel. 51

Figure 8.3. Partial unblinding in electron channel, the average value of $m_{Q_{had}}$ and $m_{Q_{lep}}$ up to 350 GeV. 53

Figure 8.4. Average invariant mass of Q in muon (top) and electron (bottom) channels. 54

Figure 8.5. Limit with 95% confidence level for electron channel only. 55

Figure 8.6. Limit with 95% confidence level for muon channel only. 55

Figure 8.7. Obtained Limit for b-veto case with 95% confidence level for electron channel only. 57

Figure A.1. Plots are obtained in muon channel, top left plot shows jet multiplicities after Cut 20 and applied W+jet reweighting, bottom left plot shows the same distribution before the W+jet reweighting and Cut 20. Top right plot refers the leading jet P_T distribution after loose analysis and bottom right plot shows b-jet weighted jet multiplicities. 60

Figure A.2. Plots are obtained in muon channel, reconstructed hadronic W mass, $\Delta\phi$ between the leading jet and E_T^{miss}, ϕ distributions of the leading jet, reconstructed leptonic W mass. 61

Figure A.3. Plots are obtained in electron channel, top left plot shows jet multiplicities after Cut 20 and applied W+jet reweighting, bottom left plot shows the same distribution before the W+jet reweighting and Cut 20. Top right plot refers the leading jet P_T distribution after loose analysis and bottom right plot shows b-jet weighted jet multiplicities. 62

Figure A.4. Plots are obtained in electron channel, reconstructed hadronic W mass, $\Delta\phi$ between the leading jet and E_T^{miss}, ϕ distributions of the leading jet, reconstructed leptonic W mass. 63

Figure B.1. P_T and η of electrons, P_T of jets, E_T^{miss} distribution in electron channel only with 3 jets. 64

Figure B.2. P_T and η of muons, P_T of jets, E_T^{miss} distribution in muon channel only with 3 jets. 64

Figure B.3. P_T and η of electrons, P_T of jets, E_T^{miss} distribution in electron channel only with 2 jets. 65

Figure B.4. P_T and η of muons, P_T of jets, E_T^{miss} distribution in muon channel only with 2 jets. 65

Figure B.5. P_T and η of electrons, P_T of jets, E_T^{miss} distribution in electron channel only with 1 jet. 66

Figure B.6. P_T and η of muons, P_T of jets, E_T^{miss} distribution in muon channel only with 1 jet. 66

LIST OF TABLES

Table 2.1. Fundamental Forces. 4

Table 3.1. LHC operations 2010 - 2012. 9

Table 5.1. $Q\bar{Q}$ production cross sections for $\sqrt{s} = 8$ TeV. 25

Table 6.1. Event preselection cut list. 32

Table 6.2. CA coefficients derived for different number of jets after loose analysis. 41

Table 6.3. Preselection yields. 41

Table 6.4. $t\bar{t}$ sample cut flow in electron channel with loose cuts. 42

Table 7.1. Summary of energy smearing and scaling for physics objects. . . . 43

Table 7.2. Standard Deviations for CA normalization factors. 47

Table 7.3. Systematic uncertainties for leptons, calculated after final selection, uncertainties are given in % both for electron channel and muon channel separately. 48

Table 7.4. Jet uncertainties calculated after final selection, uncertainties are given in % both for electron channel and muon channel separately. 49

Table 8.1. Final selection yields. 52

Table 8.2. $t\bar{t}$ sample cut flow in electron channel with tight cuts. 58

LIST OF SYMBOLS

b, $\bar{b}$	Bottom Quark
c, $\bar{c}$	Charm Quark
d_0	Transverse distance between track and the beam axis
d, $\bar{d}$	Down Quark
E_T^{miss}	Missing Transverse Energy
E_T	Transverse Energy
e, $\bar{e}$	Electron
H	Higgs Boson
j	Jet
l	Lepton
L	Luminosity
M, m	Mass
$m_{Q_{had}}$	Hadronically reconstructed Q boson mass
$m_{Q_{lep}}$	Leptonically reconstructed Q boson mass
$m_{W_{had}}$	Hadronically reconstructed W boson mass
$m_{W_{lep}}$	Leptonically reconstructed W boson mass
P_T	Transverse Momentum
p	Proton
q	Quark / Quark Field
Q	Heavy Quark Candidate
Q_{had}	Hadronically reconstructed Q quark
Q_{lep}	Leptonically reconstructed Q quark
R	Radius Of a Particle Cone
s, $\bar{s}$	Strange Quark
t, $\bar{t}$	Top Quark
u, $\bar{u}$	Up Quark
$W^{\pm}$	W Minus and Plus Bosons
W	W Boson

W_{lep}	Leptonic W
W_{had}	Hadronic W
z_0	Longitudinal distance between track and the beam axis
Z	Z Boson
ϕ	Azimuthal Angle
σ	Expected Heavy Quark Width
θ	Polar Angle
η	Pseudo-rapidity

LIST OF ACRONYMS/ABBREVIATIONS

ALICE	A Large Ion Collider Experiment
ATLAS	A Toroidal LHC Apparatus
BSM	Beyond The Standard Model
CERN	European Organization for Nuclear Research
CMS	The Compact Muon Solenoid
CP	Charge Parity
CSC	Cathode Strip Chamber
EM	Electromagnetic
EF	Event Filter
FCAL	Forward Calorimeter
GRL	Good Run List
HCAL	Hadronic Calorimeters
HEC	Hadronic End Cap Calorimeter
HLT	High Level Trigger
ID	Inner Detector
JES	Jet Energy Scaling
JVF	Jet Vertex Fraction
LAr	Liquid Argon
LB	Luminosity Block
LHC	Large Hadron Collider
LHCb	Large Hadron Collider beauty
LINAC	Linear Particle Accelerator
MC	Monte Carlo
MDT	Monitored Drift Tube
MS	Muon System
LO	Leading Order
NLO	Next-To-Leading Order
NNLO	Next-to-Next-To-Leading Order

PDF	Parton Distribution Function
PV	Primary Vertices
QCD	Quantum Chromodynamics
QED	Quantum Electrodynamics
ROI	Region of Interests
RPC	Resistive Plate Chamber
SCT	Semi-Conductor Tracker
SM	Standard Model
TDAQ	Trigger And Data Acquisition
TGC	Thin Gap Chamber
TRT	Transition Radiation Tracker

1. INTRODUCTION

Understanding the structure of matter has been one of the most astonishing puzzle about the universe and life since ages. Each answer that people discovered has fed the curiosity for knowing the smaller. With this desire, many effort has been made so far. Today, we are witnessing some of the most exciting moments of this search thanks to the Large Hadron Collider (LHC), the world's most powerful accelerator.

The elementary particles that are constituent of the known matter and the interactions between them have been understood and explained theoretically by the Standard Model of particle physics (SM). The experiments have perfectly confirmed essentially all of the theoretical predictions of the SM. Recently, the LHC has announced that the last missing piece of the SM, the Higgs boson, has been found, completing the SM. However, there are still unanswered questions about the world of particles, which require going beyond the Standard Model. Therefore, both the theoretical and the experimental studies are ongoing.

Fortunately for us, experimentalists, we have already accumulated a large amount of LHC data. In this study, the search for a new particle beyond the Standard Model is presented. The aim is to find out that whether a new heavy quark exists up to a certain mass value and set limits on its possible cross section as our available statistics permit.

2. THEORETICAL MOTIVATION

This chapter aims that to give a brief theoretical motivation for the searches of heavy quarks in the lepton+jets channel. Firstly, the Standard Model is described by explaining the fundamental particles and their interactions. Then the limitations of the SM are discussed so that the reasons for the new physics searches can be put into perspective. Finally, some models predicting the presence of new heavy quarks searches are presented.

2.1. Standard Model

What the universe is made of, how the fundamental particles interact with each other and how they can exist together have been discussed for so many years. To answer these questions, physics models were built with the existing knowledge of their time. With the accumulation of experimental results, these models were either improved or refuted but the fact is that each trial has been way better than the previous one.

Currently, the Standard Model can provide answers to many questions not only theoretically but also experimentally. All of the missing pieces have been explored with the experimental results. In this view, SM had been found to be a quite solid and complete model which can represent both the elementary particles and their interactions with each other.

2.1.1. Fundamental Particles

Standard Model is composed of 61 particles in total; 12 leptons, 36 quarks, 12 mediators and the Higgs boson (Figure 2.1). According to the current view, all matter and antimatter are made out of these particles. Quarks and leptons come in 6 different flavors each, organized into 3 families. Each quark also carries a color out of the possible three colors, so the 6 different flavors of quarks turn out to 18 particles with color charge. Both quarks and leptons have also their antiparticles; which double their numbers. The

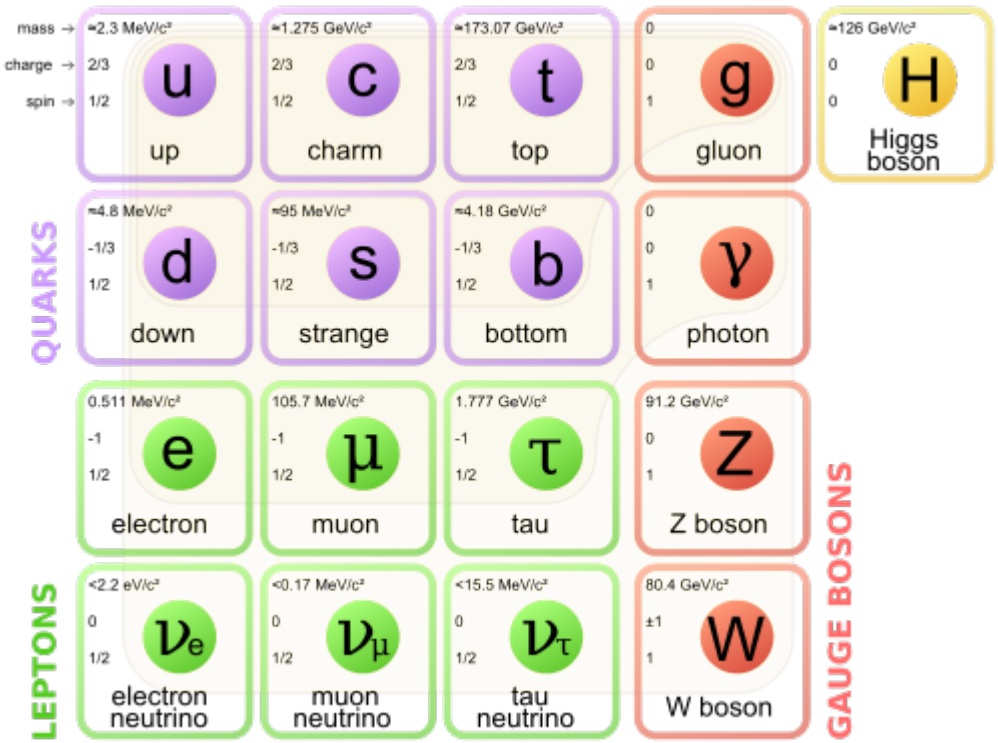

Figure 2.1. Fundamental particles [1].

interactions between these particles can be called forces and their mediators are force carriers. $W^{\pm}$ and Z bosons are three mediators for the weak force and eight colored gluons are for the strong force. Finally photons are for the electromagnetic force. These particles and their classifications can be found in Figure 2.1.

All these particles are also classified into two according to their spin quantum numbers, whether they have integer spin or half integer. Quarks and leptons have spin 1/2, hence they are fermions. The spin of photon, $W^{\pm}$ and Z are 1 and they are called bosons. Finally, Higgs boson whose spin is 0 is a scalar fundamental particle whose field is responsible for the masses of all these particles.

2.2. Fundamental Forces

Four fundamental interactions are identified in the universe so far. They are strong force, electromagnetic force, weak force and gravity. Properties of these forces are quite different in terms of their strength and the ranges. All of the information can

be seen in Table 2.1.

Table 2.1. Fundamental Forces.

Force	Strength	Range	Particles
Strong	10^{38}	10^{-18}	Gluon
Electromagnetic	10^{36}	∞	Photon
Weak	10^{25}	10^{-18}	W and Z bosons
Graviton	1	∞	Graviton

Each of the forces is carried by its mediator particle as mentioned in Section 2.1.1; with photons, gluons, W and Z bosons. These mediator particles for three fundamental interactions have been already understood theoretically and observed experimentally. These interactions are governed by the specific theories and rules; the quantum chromodynamics (QCD) for strong interactions, quantum electrodynamics (QED) for electromagnetic interactions and weak theory or flavor dynamics for the weak interactions. QED and weak theory have been well understood and are unified as electroweak theory. However, the mediator for the gravitational force, graviton is still missing and not understood. It simply waits to be discovered.

2.3. Limitations of Standard Model

While the SM is considered a complete and confirmed model especially after the discovery of the Higgs boson, it has still some shortages and limitations such as CP violation, hierarchy problem, dark matter, graviton, neutrino masses and so on. Detailed information for these subjects can be found in the literature easily. However, in the next paragraph, some of the relevant concepts with this study can be seen with their brief descriptions.

2.3.1. CP Violation

CP violation is basically the violation of the CP symmetry. CP refers charge conjugation and parity operators in the particle physics. When these operators are applied to a particle, they reverse the charge and parity features. It was thought that

CP symmetry is conserved in each process, however studies have shown that there are process that violates CP symmetry. The dominance of matter over antimatter in the present universe is result of this violation. Therefore understanding CP violation can provide a significance answer for existed matter-antimatter asymmetry.

2.3.2. Hierarchy Problem

Hierarchy problem can be seen as the huge difference between the weak scale and gravitational scale, which is a result of the non-zero Higgs field [2].

2.4. Heavy Quark Searches Beyond the Standard Model

There are various new physics models suggested for solving the limitations of the SM (Section 2.3) such as supersymmetry (SUSY), extra dimensions, new gauge bosons etc. All of these searches are still ongoing in LHC by analyzing the signatures of these models. Heavy quarks are one of the attractive signatures of the new physics in LHC. For instance, the models that predict the heavy quarks can be an explanation for the CP violation or hierarchy problem. On the other side, LHC paves the way for studying top physics by providing rich statistics for top quarks. This experience and knowledge coming from the top physics studies makes the heavy quarks searches easier. Therefore, many analysis have been already done with the possible decay channels of the heavy quarks.

The dominant production mechanism of the heavy quarks is expected to be pair production via the strong interaction up to 1 TeV. Figure 2.2 shows some of the production channels for heavy quarks. In the quark mass range from 175 to 1000 GeV, the expected cross-section for these processes at the LHC is given in Figure 2.3.

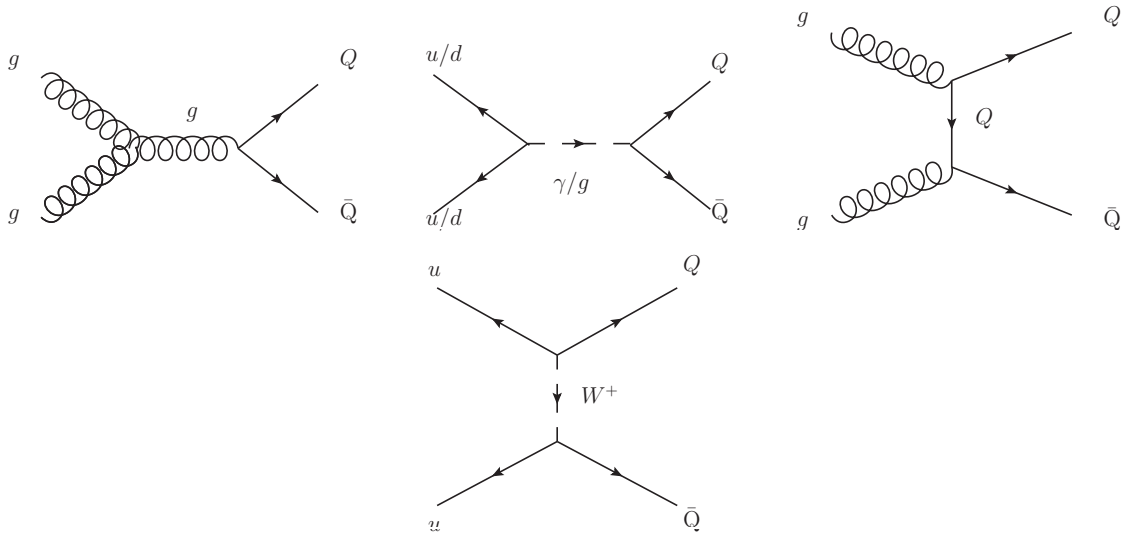

Figure 2.2. Possible tree-level SM-like production channels of heavy quarks.

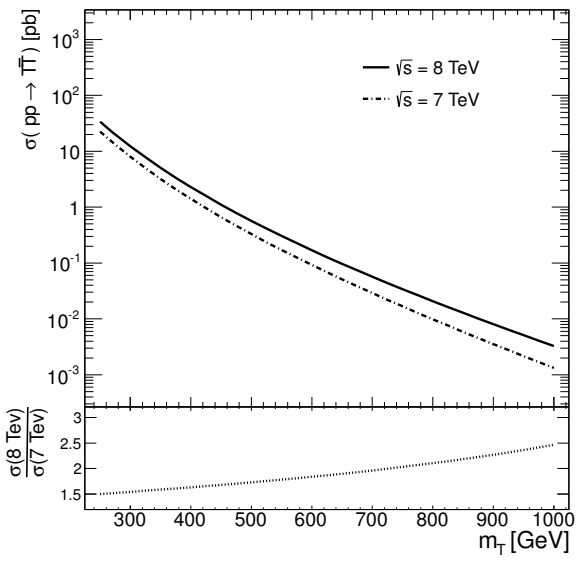

Figure 2.3. Theoretical cross sections at NNLO for $Q\bar{Q}$ production in pp collisions at two center-of-mass energies, $\sqrt{s} = 7$ TeV and $\sqrt{s} = 8$ TeV, computed by HATHOR [3].

Many studies have a tendency to assume that these new heavy quarks can decay into a W and a third generation quark with 100% branching ratio. However this assumption is only caused by the current knowledge about the mixing patterns of the discovered quarks. In this study, heavy quarks can also mix with the light quarks which are u, d, c or s. There are also some models, which allow only decays to the first generation quarks.

3. THE ATLAS EXPERIMENT

This chapter briefly introduces the Large Hadron Collider (LHC) and the ATLAS detector. The main goals of the ATLAS experiment are explained together with the nomenclatures that are necessary for the reader to be able to follow the discussion. Each of the components of the ATLAS detector, starting from the tracking system to the calorimeters and the muon system are described with separate sections. Lastly, to give a complete view of the experiment, data acquisition system and trigger are also presented.

3.1. LHC

The Large Hadron Collider (LHC) is one of the most fabulous scientific and technological achievements of humanity with a higher center of mass energy than has ever been explored at any previous collider. It is a two-ring superconducting hadron accelerator, located in 26.7 km long LEP tunnel that lies between 45 m and 170 m below the surface around the France-Switzerland border [4]. European Organization for Nuclear Research (CERN) is executing this project with the support of many countries and institutions since 1994 to study both the Standard Model and the physics beyond the Standard Model with the center of mass energy of up to 14 TeV. Although the accelerator was designed to observe mainly proton-proton (pp) collisions, ion beam collisions are also operated in the accelerator for a specific periods.

Commissioning of the LHC started by the end of the 2009. From then, until the end of the 2011, it was operated at a center of mass energy of 7 TeV (Table 3.1), mainly to gain enough confidence about the machine protection system and to explore the limits of the machine itself. In 2012, with the center of mass energy of 8 TeV, LHC successfully collected 23.1 fb^{-1} data and enabled the discovery of Higgs boson [5]. After three years of operation (Run I), LHC has stopped for upgrade and maintenance studies (LS1) to be able to perform at center of mass energy of 13 TeV as targeted in 2015.

Table 3.1. LHC operations 2010 - 2012.

Year	Overview	COM energy	Integrated Luminosity $[fb^{-1}]$
2011	Commissioning	7 TeV	0.04
2011	Exploring limits	7 TeV	6.1
2012	Production	8 TeV	23.1

On the LHC ring, there are four main detectors to explore the high energy beam collisions. ATLAS and CMS are general purpose detectors, designed for high luminosity data collected with proton beams of a luminosity of up to $L = 10^{34}$ cm^{-2} s^{-1}. To study B-physics, there is LHCb with a lower luminosity aim of $L = 10^{32}$ cm^{2} s^{1}. Lastly, for the heavy ion experiments, ALICE detector is operated with the luminosity of $L = 10^{27}$ cm^{-2} s^{-1}.

This study is performed with the ATLAS detector, therefore detailed explanations about the ATLAS detector can be found in the following sections.

3.2. THE ATLAS DETECTOR

ATLAS (A Toroidal LHC ApparatuS) Experiment performed by a collaboration of around 3000 physicists from over 175 institutions in 38 countries. The detector itself is as big as the collaboration; it is 44 meters long, 25 meters in height and weight of the detector is about 7000 tonnes (Figure 3.1)[1].

3.2.1. Coordinates and Nomenclatures

In the ATLAS detector, nominal interaction point is accepted as the origin of a right handed coordinate system and the beam direction defines the z-axis. According to this, the x-y plane is the plane transverse to the beam direction; x-axis points from the interaction point to the center of the LHC ring and the y-axis points upwards. The side with positive z is called the A side and the other side with negative z values is C side. Unless stated otherwise, all the transverse variables such as P_T, E_T and the missing energy E_T^{miss} are all defined in the x-y plane.

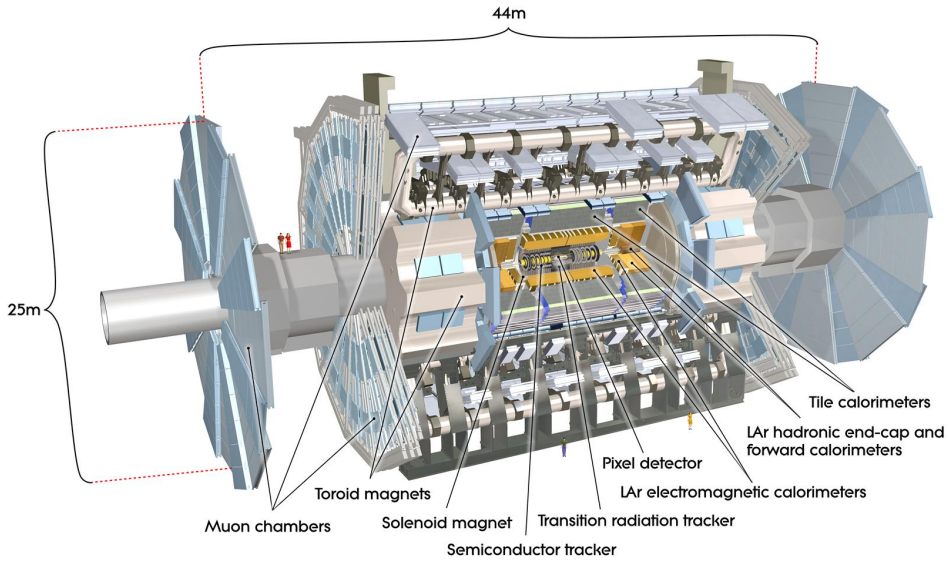

Figure 3.1. Atlas Detector [4].

The azimuthal angle ϕ is measured around the beam axis, and the polar angle θ is the angle from the beam axis. The pseudorapidity, which is used to describe the angle of a particle relative to the beam axis is defined as $\eta = -\ln\tan(\theta/2)$. The distance ΔR in the pseudorapidity-azimuthal angle space is defined as $\Delta R = \sqrt{\Delta\eta^2 + \Delta\phi^2}$.

Five helix parameters are used to describe the trajectories of the charged particles in ATLAS. In x-y plane; $\frac{1}{P_T}$, ϕ and transverse impact parameter (d_0) that is defined as the transverse distance to the beam axis at the point of closest approach; signed according to the reconstructed angular momentum of the track about the axis. In the R-z plane; $\cot\theta$ and longitudinal impact parameter (z_0) which is the z coordinate at the of the point of closest approach.

3.2.2. Inner Detector and Tracking

The innermost part of the ATLAS detector, the Inner Detector (ID), is mainly responsible for the tracking system, vertex identification and momentum measurements of the charged tracks within the pseudorapidity range $|\eta| < 2.5$ and above a certain P_T threshold. It is located around the beam pipe and inside a solenoidal magnetic field of 2 Tesla. The outer radius of the ID cavity is 115 cm and its length is about

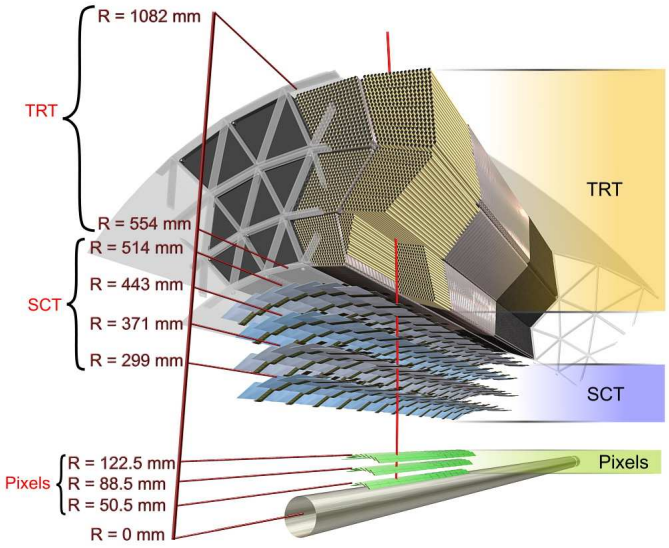

Figure 3.2. Inner Detector [4].

7 m. (Figure 3.2) It has three subdetectors which are from the inside out the pixel detector, semiconductor tracker (SCT) and the transition radiation tracker (TRT) respectively. They are placed around the beam axis concentrically in the barrel region and perpendicular to the beam axis in the end-cap regions on disks .

3.2.2.1. Pixel Detector. Considering the requirements of the targeted physical processes in ATLAS, it is possible to understand the necessity of performing high-precision measurements in detectors. To achieve that, fine granularity is required and pixel detector provides the highest granularity around the vertex region. High-resolution pattern recognition is achieved by discrete space points from silicon pixel layers crossed by each charged track. Pixel layers consist of identical pixel sensors with minimum pixel size in $R - \phi \times z$ of 50x400 μm^2 and have 80.4 million readout channels [4]. Barrel and both end-caps have a total of 1744 modules. Pixel detector is the most important contributer in achieving a small impact parameter resolution and in identifying short-lived particles such as B hadrons and τ leptons.

During the Run I, pixel detector had three barrels at radii of 50.5 mm, 88.5 mm and 122.5 mm. However, with the increasing center of mass energy in run 2, better performance of the detectors is required. Therefore, an extra silicon pixel detector,

which is called inserted B layer (IBL), at 32 mm from the beamline is also being inserted to the pixel detector during LS1 [6]. With the IBL, it is expected that the detector performance will be increased much in terms of vertexing performance, b tagging efficiency and searches of B physics.

3.2.2.2. Semiconductor Tracker. Semiconductor tracker (SCT) is placed in the middle of the ID, between the pixel detector and TRT. It contributes to the measurement of momentum, impact parameter and vertex position. In the barrel region, SCT has four cylindrical layers that consist of 2112 modules at radii of 299, 371, 443 and 514 mm. In the end caps, there are 9 disks with 1976 modules. Each module has 4 silicon sensors, two each on the top and bottom side. Sensors are made from p-type silicon 80 μ m pitch microstrips implanted on n-type wafers aligned with a stereo angle of 40 mrad. This angle simplifies the geometry and increases the efficiency of track identification. These eight layers of silicon microstrip detectors provide precision points in the R-ϕ and z coordinates [4]. SCT has 17 μm nominal resolution in plane lateral (R-ϕ) and 580 μm in plane longitudinal (z or R).

3.2.2.3. Transition Radiation Tracker. The outer-most region of the ID is the transition radiation tracker (TRT) which consists of 4 mm diameter straw tubes filled with the nonflammable gas mixture of Xe, CO_2 and O_2. Each straw tube has an anode sense wire at their center to create high voltage difference with respect to the straw tube wall that serves as cathode, so that charged particles can ionize the gas as they pass through inside the tubes. Ionized gas is collected and converted to electrical signals. Using the information of arrival times of the ionized pairs, hits can be generated in TRT.

Due to the high cost of the materials used in the SCT and pixel detectors, precision layers are limited to three pixel layers and eight strip layers which are crossed by each track. On the contrary, TRT identifies large number of tracking points, about 36 per track, providing continuous track following up to $|\eta| < 2.0$ with much less material per point and a lower cost. Lower precision of the TRT hits is compensated by

the large number of measurements and TRT contributes significantly to the momentum measurements, electron identification and especially for the detection of photon conversions and V0 decays [3].

In the barrel region, TRT has 50000 straws which are parallel to the beam axis while in the end-caps there are 320000 straws arranged radially in wheels. Each straw gives 170 mm spatial resolution in R-ϕ plane with 420000 electronic channels. The drift-time information coming from the each electronic channel is used for the discrimination between the transition radiation hits and tracking hits.

3.2.3. Calorimeters

The ATLAS calorimeters are placed in between of the ID and MS and they are outside of the 2 T solenoid magnet. The main task of the calorimeters is to measure the energy of the incoming particles. There are two types of calorimeters in ATLAS; hadronic and electromagnetic (EM) calorimeters. They are all sampling calorimeters meaning that they are composed of different materials as active material and absorber material. Similar to the subdetectors of ID, they have separate parts in the barrel region and in the end caps as can be seen in Figure 3.3. Calorimeters provide a large η coverage, $|\eta| < 4.9$, and the thickness of the calorimeters is well determined for preventing a punch through of jets into the muon system and maximizing the containment of both the electromagnetic and hadronic showers.

3.2.3.1. Electromagnetic Calorimeter. Electromagnetic calorimeters are responsible for the energy measurements of the electromagnetically interacting particles such as electrons, positrons and photons. These particles can interact with the matter with various ways creating the electromagnetic showers. For energies above 100 MeV, electrons and positrons they lose their energy almost entirely through bremsstrahlung creating energetic photons. For the photons, the major interaction is pair production, which gives another energetic electron or photon [8].

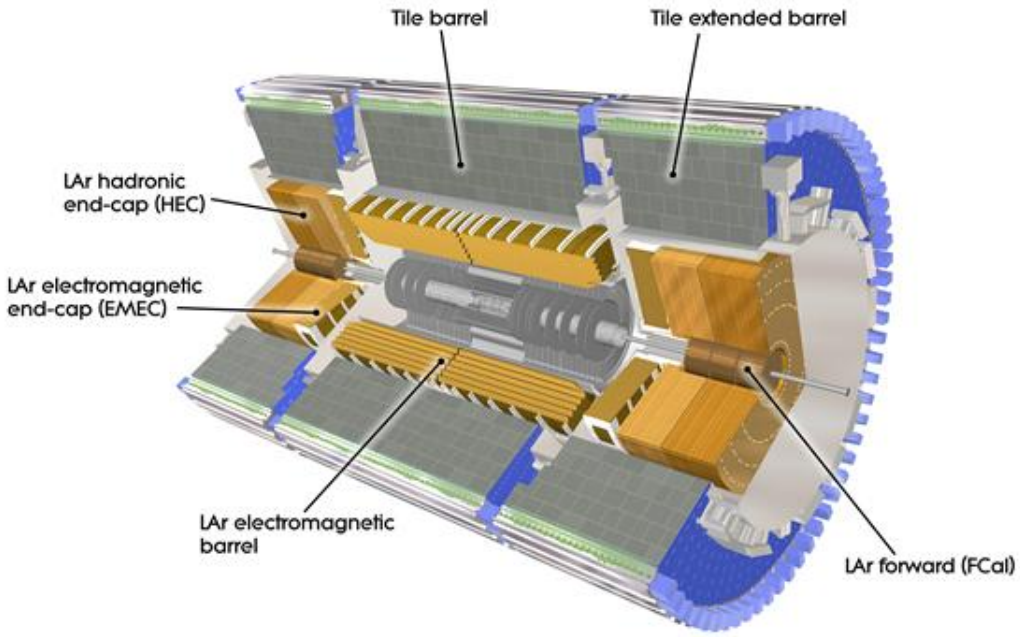

Figure 3.3. ATLAS Calorimeters [4].

In the ATLAS detector, the electromagnetic calorimeter is a lead-liquid argon (LAr) detector which uses LAr as active material and lead as absorber. The shape of the EM calorimeter is similar to the geometry of an accordion to gain a complete and uniform coverage. Its pseudorapidity range is $1.375 < |\eta| < 3.2$ in the two end caps and $|\eta| < 1.475$ in the barrel region. The thickness of the calorimeters is > 22 radiation lengths (X_0) in the barrel region and $> 24X_0$ in the endcaps preventing a punch through of jets into the muon system [4]. While the regions matched to the ID can provide precision measurements of electron and photons with the fine granularity of EM in these regions; the rest plays significant role for jet reconstruction and E_T^{miss} measurements.

3.2.3.2. Hadronic Calorimeter. The hadronic calorimeters (HCAL) measure the energy of strongly interacting particles such as $\pi^{\pm}$, $K^{\pm}$, K^0, protons and neutrons. As a standard detector design, hadronic calorimeter is placed behind the EM calorimeter to be able to absorb the energy of hadronic showers which is much greater than the electromagnetic showers.

HCAL is divided into three different parts. The first is the tile barrel region up to $|\eta| = 1.0$, the second is the extended barrel region with $0.8 < |\eta| < 1.7$. The iron is used as absorber and the active material is scintillating tiles. Particles passing through the scintillating tiles produce light proportional to the incident energy which specifies the read-out signal. Second part is the hadronic end-cap (HEC) calorimeter. It is a copper- Liquid Argon (LAr) sampling calorimeter with a coverage of $1.5 < |\eta| < 3.2$. In the very forward region, providing a large η coverage to calorimeters, the forward calorimeter (FCAL) is installed in the region of $3.1 < |\eta| < 4.9$. FCAL uses copper and tungsten as absorber material and it measures the EM component of very forward jets.

3.2.4. Muon Chambers

The muon spectrometer (MS) is the outermost part of the ATLAS detector. It is composed of three large superconducting air-core toroid magnets, a trigger system and high-precision tracking chambers. MS is responsible for the detection of charged particles escaping the calorimeters and measuring their momentum in the pseudorapidity region up to $|\eta| < 2.7$. It has three concentrical cylindrical layers around the barrel region with radii 5 m, 7.5 m and 10 m and two large wheels in the end-cap regions with their own end-cap toroid magnets. There are three toroid magnets, one is located in the barrel region and the other two is in the endcaps as just mentioned. The barrel toroid provides 1.5 to 5.5 Tm of bending power in the range of $0 < |\eta| < 1.4$, and the end-cap toroids approximately 1 to 7.5 Tm in the region $1.6 < |\eta| < 2.7$ [4]. These magnets create a non-uniform magnetic field so that particles trajectories are bent in the MS with respect to their P_T, allowing to measure their P_T with about %10 resolution. There are four different type of detectors in the MS. Monitored Drift Tubes (MDT) and Cathode Strip Chambers (CSC) are used for high precision tracking. MDTs are cylindrical drift tubes filled with a gas mixture of Ar and CO_2. They cover the pseudorapidity region of $2 < |\eta|$. Over the region of $2 < |\eta| < 2.7$, with a higher granularity, CSC are active, providing higher rate capacity and better time resolution. CSC are multiwire proportional chambers whose cathodes are segmented into strips to

provide full 3D space points. Resistive Plate Chambers (RPC) and Thin Gap Chambers (TGC) are used for triggering on the events with muons. Their response time is shorter comparing to the other two detector. RPCs are gaseous tracking chambers composed of two resistive parallel plates. Creating an electric field between the plates, an avalanche is created when a muon enters the region. The space–time resolution is about 1 cm $\times$ 1 ns with digital readout. Triggering in the end caps is done by TGCs with 4 ns time resolution. RPCs and TGCs are not only used for triggering, they also provide bunch-crossing identification, well-defined P_T thresholds and contribute to the measurements done for the muon coordinates.

3.2.5. Trigger and data acquisition

ATLAS could achieve $7.73 \times 10^{33} cm^{-2} s^{-1}$ peak luminosity in Run 1. Since the total number of collision is so high in the LHC, it is not possible to record each event to disks. That is why, ATLAS trigger system decides whether an event carries significant information for the ongoing physics analyses or not and then it records only the desired ones.

During Run 1, ATLAS triggering system operated in three different trigger levels which are Level 1 (L1), Level 2 (L2) and Event Filter (EF) triggers. L2 and EF are together called the High Level Trigger (HLT). For Run 2, removing the separation between L2 and EF, number of trigger levels will decreased to 2, L1 and HLT.

L1 trigger is a data acquisition hardware system. It operates in runtime to look for pre-defined physics signatures by using the information coming from the calorimeter and muon systems. It also defines a region of interest (ROI) in the detector that carries the information of the accepted objects, their location and the relevant threshold information. L1 reduces the output event rate to about 75 kHz and has a latency of 2.5 μs and then forwards the accepted events to the L2 trigger.

L2 and EF are both software systems that can access to the detailed information related to the events. In L2, objects can be reconstructed based on the information

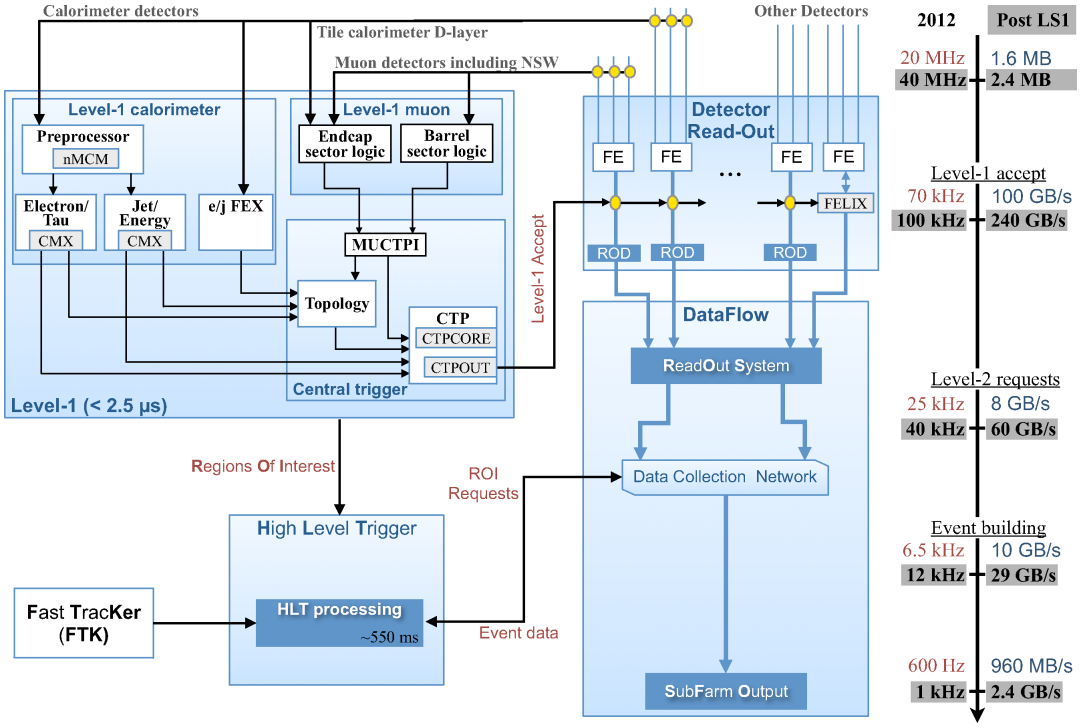

Figure 3.4. Schematic overview of the Trigger and DAQ system [7].

coming from the specific ROIs using simple algorithms. The output rate of L2 is 3.5 kHz and average decision time is about 40 ms.

EF trigger uses more complex algorithms like the offline reconstruction algorithms. It uses the complete detector information to be able to make the final selection and reduce the final rate to about 200 Hz with an event size of approximately 1.3 MByte [4].

4. PHYSICS OBJECTS

Although designing and constructing a successful detector is crucial for the high energy physics experiments, correct interpretation of the detector signatures as physics objects can be considered equally important. In the ATLAS detector, different procedures and methods are used for reconstructing each physics object.

In this analysis, final state physics objects are electrons, muons, jets and missing transverse energy. In this regard, this chapter describes the reconstruction of these objects together with the information about the calibration processes and identification criteria in the ATLAS experiment. Since the signals of this search are heavy quarks, the analysis strategies are expected to be similar to a top quark analysis. Therefore, all the object definitions are done according to the ATLAS Top group recommendations and criteria.

4.1. Electrons

Electrons are charged particles whose tracks can be identified by the ID as explained previously and energies can be measured from the clusters in the electromagnetic calorimeter. In ATLAS, the method of the electron reconstruction is basically the association of a a well-reconstructed charged particle track to a proper cluster in the electromagnetic calorimeter. Although electrons can lose some amount of their energies in the ID due to the bremsstrahlung processes; it is possible to fit electron tracks in such a way as to account for bremsstrahlung with the proper recovery algorithms [9].

Association starts with the formation of the EM clusters by using the sliding window approach, where the window size is 3×5 in η/ϕ middle layer cell units of 0.025×0.025. After removing the duplications and elimination of the clusters whose energies are below 2.5 GeV, candidate clusters are identified. If there is at least one qualified track [9], the track with silicon hits and the one with the smallest ΔR is preferred and then cluster becomes an electron candidate. The energy of the electron

is given by the cluster energy while the ϕ and η directions are taken same as the corresponding track parameters at the vertex.

An additional step for electron identification is the isolation requirement. To remove background, candidates are required to be isolated from additional energy deposits in the calorimeter. If the amount of the energy deposition within a narrow cone about the electron axis is large, the candidate is rejected. For the semileptonic c and b quark decays, the lepton would be collimated increasingly close to the jet coming from the associated quark as the P_T of the quark increases. In this case, it is possible to decrease the radius of the isolation cone by increasing the electron P_T cut values so that the efficiency of the selection can be preserved.

Although the selection and identification criteria can be individually modified according to the different requirements of each physics analysis, ATLAS specifically provides a couple of well-defined sets of electrons for generic use in analyses. The detailed information of the ATLAS electron identification criteria can be found in the associated paper [10]. In general, this study follows the ATLAS top physics group recommendations. Based on these recommendations, two sets of electrons are selected in the analysis level with different criteria, on top of the ATLAS selections. First group is the loose electrons that are chosen for the estimation of the background events. The other group is tight electrons whose selection criteria are more stringent than the loose ones. This group is the main set for the analysis, meaning that the final state lepton is selected out of these tight electrons.

4.1.0.1. Loose Electrons.

- Electrons are selected out of the medium electrons defined in reference [11].
- The distance between the primary vertex (PV) and the initial point of the track in the beamline has to be close, satisfying $|z_0 - z_{PV}| < 2mm$.
- Electrons should satisfy $P_T > 25$ GeV.
- Electron candidates are required to be in the $|\eta| < 2.47$ region and the cluster

should be outside of the crack region $1.37 < |\eta| < 1.52$.

4.1.0.2. Tight Electrons. Applying the same selection criteria as applied to the loose electrons, the tight electrons should also fulfill the isolation requirements within both the calorimeter and the tracker.

- Isolation: The total E_T in a cone of opening 0.2 around the electromagnetic cluster's centroid, minus the electromagnetic cluster E_T, has to be below than 6 GeV. Working point is selected as 90%. Same logic also applies for P_T cones.

4.2. Muons

ATLAS provides a wide range of options for muon identifications. There are various muon reconstruction algorithms that differ from each other according to the detector participation. Additionally, there are different quality requirements for muons which is useful to estimate the different level of backgrounds in any analysis. Currently, there are four reconstruction algorithms that define the muon types: MS-standalone, combined, segment-tagged and calorimeter-tagged. Based on the recommendations of the top physics group, combined muons are used in this analysis. Therefore, it may be convenient to explain the underlying algorithm for this type of muons here.

Combined (CB) muons are reconstructed from the information coming from two detector parts; ID and MS. ID and MS both have different tracking mechanisms and they can provide their own tracks independently. After ID and MS tracks are reconstructed, a comparison between the two sets of tracks is performed and from the successful matches, combined tracks are produced. By using combined tracks, combined muon candidates can be reconstructed with highest muon purity among the other type of muons [12]. Candidate muons are also required to satisfy certain threshold values for P_T and η and they all should fulfill the track quality requirements. Apart from the energy isolation criteria, muons have to satisfy P_T dependent isolation requirements.

In this study, muon identification is done for two set of muons similar to the electrons. Loose muons are used for the background estimation and tight ones are for the final event selections [12].

4.2.0.3. Loose Muons.

- Muons are required to be combined.
- They must be within the detector acceptance $|\eta| < 2.5$.
- Muons should satisfy $P_T > 25$ GeV.
- Muons must pass the MCP ID track quality cuts [12].
  - (i) Number of pixel hits + number of crossed dead pixel sensors > 0.
  - (ii) Number of SCT hits + number of crossed dead SCT sensors ≥ 5.
  - (iii) Number of pixel holes + number of SCT holes < 3.
  - (iv) In the region of full TRT acceptance for $0.1 < |\eta| < 1.9$ at least 9 TRT hits.
- The distance between the primary vertex and the initial point of the track in the beamline has to be close satisfying this relation $|z_0$ wrt $z_{PV}| <2$ mm.
- Overlap removal between the jets and muons is necessary with satisfying the relation $\Delta R(m, j) > 0.4$, where j is any jet with $P_T > 25$ GeV and $JVF > 0.5$.

4.2.0.4. Tight Muons. Applying the same selection criteria as the loose muons, tight muons should also fulfill the isolation requirements within surrounding momentum cones. The ratio of the summed momenta of all tracks with a cone except the muon track itself to the momentum of the muon, $\frac{P_T cone}{P_T} < 0.05$.

4.3. Jets

As it has already been stated in Chapter 2, quarks and gluons can not exist freely since they are colored particles. In high energy physics experiments, they can be recognized as jets, from the energy depositions they left in the calorimeter after being fragmented and hadronised.

There are various jet reconstruction algorithms using either tracks, topological clusters, cells or calorimeter towers as seeds. In this analysis, all jets are reconstructed using the Anti-Kt algorithm [26] with distance parameter R = 0.4. In this method, inverse of the transverse momentum with respect to the beam axis is used to weight energy depositions in the clustering. Topological clusters are used as inputs.

All jets are calibrated to the hadronic energy scale using a correction factor obtained from simulation which depends on P_T and η. Reconstructed jets are required to satisfy $P_T > 25$ GeV and $|\eta| < 2.5$. Jet reconstruction efficiency is nearly 100 % [29].

Furthermore there is an additional parameter for jets to define their quality, Jet Vertex Fraction (JVF). This variable refers to the fraction of tracks coming from the primary vertex inside the reconstructed jet. By requiring a high JVF, the probability of choosing a jet coming from the primary pp interaction is increased since the tracks coming from pile up collisions are unlikely to contribute to the reconstructed jets in this case. Therefore, jets are also required to satisfy $JVF > 0.5$.

Lastly, to decrease the misidentification between muons and jets, an overlap removal procedure should be performed. Since analysis considers also fake contributions, overlap removal procedure is applied separately for both loose and tight muons.

4.4. Missing Transverse Energy

In the LHC protons are accelerated along the z axis. Therefore, from the law of conservation of momentum, the vector sum of all the transverse momenta should be zero since sum of the initial momenta is zero in the x-y plane. However, due to detector effects, this sum may not be zero. In order to preserve the conservation of transverse momentum, missing transverse energy (E_T^{miss}) is defined as the negative vector sum of the momenta of all the detected particles.

Since neutrinos are weakly interacting particles, direct detection is not possible with the ATLAS detector. In this case, the presence of a neutrino in an event can be

associated with E_T^{miss} in that event. Furthermore, there are BSM studies that predict new weakly interacting particles and in these studies, E_T^{miss} is an important signature for the presence of these particles [28].

Reconstruction of E_T^{miss} in ATLAS is the final reconstruction step since it requires the information coming from all the other physics objects. Firstly, calorimeter energy deposits are associated with a reconstructed and identified high-P_T objects in the following order: electrons, photons, hadronic decays of τ, jets, muons. The remaining unassociated clusters are taken into account to suppress the noise coming from pile up collisions, low P_T tracks and jets. This component is called the soft term $E_x^{miss,SoftTerm}$ and it is obtained from the topological clusters in the calorimeter.

$$E_x^{miss} = E_x^{miss,e} + E_x^{miss,\gamma} + E_x^{miss,\tau} + E_x^{miss,jets} + E_x^{miss,SoftTerm} + E_x^{miss,\mu} \qquad (4.1)$$

In Equation 4.1, each term is calculated as the negative sum of the calibrated reconstructed objects, projected onto the x and y directions. While all the terms except $E_x^{miss,\mu}$ are coming from the calorimeter, $E_x^{miss,\mu}$ may come from muon spectrometer since muon P_T values are better estimated in there.

In this thesis, one of the W bosons decays leptonically resulting in a neutrino in the final state. Therefore, it is obligatory to look for E_T^{miss} in the final selection of the events. An ATLAS software package (MissingETUtility-01-01-03) based on the above mechanism is used for reconstructing E_T^{miss}.

5. DATA, BACKGROUND AND SIGNAL SAMPLES

In this thesis, the search for pair produced heavy quarks is presented in the channel $Q\bar{Q} \rightarrow WqWq \rightarrow 4$ jets$+l+E_T^{miss}$, is presented (Figure 5.1). In order to perform the analysis, it is essential to know the relevant background processes for this channel and to use appropriate datasets. This section starts with information on the data and Monte Carlo (MC) samples used in the analysis. After that, corrections applied to the samples are explained.

5.1. Data

The search is based on the the data collected by the ATLAS detector during the 2012 Run I, with 8 TeV center of mass energy. The analyzed data corresponds to an integrated luminosity of $\int Ldt = 20$ fb^{-1}. In the ATLAS experiment, the data is recorded in different periods such that both the quality and the quantity of the data periods can be different. Collected data is processed with the ATLAS software AtlasPhysics 17.2.7.5.7.

For this analysis, the data processed for the top group is used. The format of the data is a ROOT based ntuple format known as 'ntuptop'. Its production was done in February 2013. A small amount of missing events were identified in periods I-L and these were reprocessed in October 2013 using. In this regard, this analysis uses the

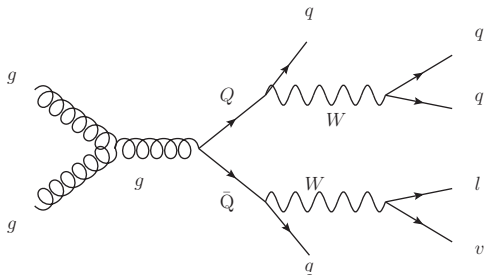

Figure 5.1. Feynman diagram of the semileptonic decay channel of the pair produced heavy quarks.

dataset containers p1400_p1401 for periods A, B, C, D, E, G, and H; p1595_p1596 for periods I, J and L. Period M is not on the good run list of the ATLAS (Section 6.1.1).

5.2. Signal Samples

The signal used in this analysis is for the t′ →Wq channel. There are 11 samples that spans the interval of heavy quark mass from 350 GeV to 900 GeV with the increases of 50 GeV in each step. The generator of the samples is PYTHIA8 [17] with AU2 tune and the parton distribution function is the MSTW 2008 LO (Leading Order) PDF set [21]. 500 GeV, 800 GeV and 900 GeV samples are produced with full simulation (FS) using GEANT4 [14], while the remaining samples are produced with fast simulation which involves GEANT4 and parametrized models of some parts of the detector, (ATLFAST2) [27]. In these samples, t′ can decay into any of the down type quarks with different branching fractions. Branching fraction to the light quark (d, s) decays are each 0.25 and to the b quark decay is 0.5.

The signal sample cross sections for $Q\bar{Q}$ production have been calculated by HATHOR [3] at NNLO (Next-To-Next-To-Leading Order) are given in Table 5.1.

Table 5.1. $Q\bar{Q}$ production cross sections for $\sqrt{s} = 8$ TeV.

m_Q(GeV)	$\sigma_{Q\bar{Q}}$(pb)
300	12.32
400	2.33
500	0.587
600	0.177
700	0.0605
800	0.0225

5.3. Backgrounds

To be able to discover a new particle, it is essential to have a well-modeled backgrounds for the Standard Model interactions since the presence of a new physics

can only be understood by a comparison between the backgrounds and the data. The backgrounds are predicted by the MC generators simulating the pp collisions in ATLAS. For this analysis, there are various background processes that can create the same final state with the $Q\bar{Q}$ events such as W+jets, $t\bar{t}$, single t samples etc. These different event samples are given in this section together with detailed information about their generators.

5.3.1. W+jets

W+Jets background is estimated from two different sets of samples. First set of samples are generated with Alpgen [15] v2.13 CTEQ61 PDF set [21], 2011C tuning and then hadronized with Pythia [17]. Second set of samples are produced with Sherpa [18] v1.4.1 using CT10 PDF set [21].

The samples generated by Alpgen are separated into different groups based on the flavor of the jets such as W+light jets, Wbb+jets, Wcc+jets, and Wc+jets. To be able to handle different contribution of the flavors, a flavor correction needs to be done to these samples. On the other hand, Sherpa samples don't require this kind of flavor correction. Therefore for this analysis, Sherpa samples are preferred as default for W+jet background estimation.

Presented results and final selections are obtained with the so-called boosted samples of Sherpa, which are divided into different groups according to the P_T of W boson. These groups are 70-140 GeV, 140-280 GeV, 280-500 GeV and 500-1 GeV. The region of 0-70 GeV is extracted from an all inclusive sample by rejecting the events with boosted W bosons at the MC level. However, Alpgen samples are also used as a control group to be able to understand W+jets background better and to see the effects of the generator.

Both samples are normalized according to the data driven method for charge asymmetry correction as it has been already explained in Section 5.4.1. Additionally, Sherpa samples are reweighted in order to improve the shape discrepancy seen in the

P_T distributions, details can be found in Section 5.4.2.

5.3.2. $t\bar{t}$ Background

$t\bar{t}$ background is one of the dominant backgrounds in this analysis since the Feynman diagram of $Q\bar{Q}$ pair (Figure 5.1) also applies for the $t\bar{t}$ pairs. The decay of the $t\bar{t}$ pair gives the same final state therefore it should be well estimated.

$t\bar{t}$ samples are generated with the Powheg [20] and Pythia [17]. The Powheg matrix element events are generated with CT10 PDF [21] at NLO (Next-To-Leading Order). The parton showering, fragmentation and hadronization is done by Pythia v2.13 with P2011C tune which uses CTEQ6L1 PDF at LO. In these samples, at least one of t and $\bar{t}$ doesn't decay to hadrons.

5.3.3. Single Top

Two different set of samples are used for the two channels of the single top background samples; t-channel and s-channel. The backgrounds in the s-channel are generated with Herwig at NLO with AUET2 tuning and CT10 PDF set. Parton shower and hadronization is performed by Herwig v6.520. The t-channel backgrounds are generated by AcerMC [19] and Pythia with AUET2B tune. The AcerMC matrix element events are generated with CTEQ6L1 (LO) PDF [21]. The fragmentation is simulated with the version 6.421 of Pythia. All single top backgrounds are full simulation samples.

5.3.4. Dibosons

ZZ, WW and WZ backgrounds, all filtered for one lepton and no additional jets are generated by Herwig [16] with AUET2 tune, CTEQ6L1 PDF set. Lepton filter requires that $P_T > 10$ GeV and $|\eta| < 2.8$. Additional samples up to three additional partons are also included the dibosons background. They are generated with the same tuning and PDF set as Alpgen+Herwig. All samples are full simulated backgrounds for the dibosons.

5.3.5. Z+jets

For the Z+jets background, two different sets of MC samples are used and compared to each other. One set is generated by Alpgen and Pyhtia with the CTEQ6L1 PDF and then soft parton showering, fragmentation and hadronization are done by Pythia. However, these samples require flavor correction like the W+jets Alpgen samples. The second set of samples are produced with Sherpa v1.4.1 [18] with the CT10 PDF. These set of samples are generated with the same method as the W+jets Sherpa samples, that is given in Section 5.3.1. Both samples are examined during the analysis. Z+jets contribution for the analysis channel is not one of the dominant backgrounds, therefore Sherpa samples can be used without any further corrections.

5.4. Data Driven Corrections and Contributions for Background

5.4.1. W+jets Charge Asymmetry Normalization

The total number of W+jets events in the data can be estimated well using the charge asymmetry measurements of the W+jets background. The amount of the produced W^+ bosons in LHC is higher than the W^- bosons and the modelling of their ratio is considered to be well modelled in the MC simulation. However, the exact amount of the W^+ or W^- in data is not known.

The ratio of the production cross sections of the W_++jets and W_-+jets is almost constant [22], where n refers to the number of jets in the events in Equation (5.1).

$$R(n) = \frac{\sigma(n\ jet + W^+)}{\sigma(n\ jet + W^-)} \tag{5.1}$$

Using this theoretical information, it is convenient to extract a data-driven normalization for the total W+jets background. The total number of W+jets (N_W) events in

data can be calculated via Equation (5.2).

$$N_W = (\frac{N_{W^+} + N_{W^-}}{N_{W^+} - N_{W^-}})_{MC} \times (N_{W^+} - N_{W^-})_{Data} \tag{5.2}$$

5.4.2. W+jets P_T Momentum Reweighting

After event preselection, a disagreement between data and MC is observed in the P_T dependent distributions both for the electron and the muon channels (Figure 6.3 and Figure 6.5). The reason of this behavior is investigated and it is understood that the quality of the P_T estimation of the simulated W+jets samples is not adequate. This assumption is tested by using different MC samples from different generators and by different analysis groups in ATLAS who use W+jets samples in their analyses as background.

In this study, both Alpgen and Sherpa samples are checked. In high P_T regime, both simulations expect more events than the collected data although their estimations are better in the lower and the middle region of the P_T range. The finding of this analysis and the other ATLAS studies agree about the level of the discrepancy. Therefore, a correction function is derived based on an exponential fit for the P_T distribution of Sherpa samples to produce a reweighting mechanism. After the fit function has been extracted, in the analysis level the procedure requires the P_T information of the reconstructed W_{lep} as input and then returns a new reweighting factor (RF) for the MC event weight which is multiplied by the original event weight.

$$RF = \exp(2.96916 \times 10^{-2} - 9.21642 \times 10^{-4} \cdot P_T^W) \tag{5.3}$$

5.4.3. Fake Contribution

Lepton misidentification can cause additional background events for analyses whose final states require leptons. Lepton misidentification can be seen in various ways

related to the quantum chromodynamical effects. There may be either non-prompt leptons or misidentified particles such as jets or photons in an event, which are called as fake leptons, and they may create significant amount of background especially when the selection criteria of the analyses are loose. Due to the large QCD cross sections and the low probability of misidentification, it is obligatory to estimate fake contribution using data-driven techniques and then add it to the expected backgrounds. For this, the so-called matrix method, which is based on the measurement of efficiencies of leptons with loose identification criteria, is commonly used.

$$N^{loose} = N^{loose}_{real} + N^{loose}_{fake}, \tag{5.4a}$$

$$N^{tight} = \epsilon_{real} N^{loose}_{real} + \epsilon_{fake} N^{loose}_{fake}, \tag{5.4b}$$

In this analysis, using an ATLAS software package (FakesMacros-00-00-45) provided by the ATLAS Top Fakes group [23], fake contributions have been calculated with the matrix method. To perform this technique, a parallel analysis is performed using loose leptons, which are already defined in Chapter 4. Comparing the number of events coming from the loose and tight lepton results, fake lepton contributions are obtained.

6. SEARCHING FOR THE NEW PARTICLE

Discriminating the signal from the background is a challenging task for the studies that predict significant amount of background events. Therefore, it is highly important to reduce the background events as much as possible without loosing the signal events. For this analysis, event selection is done so as to have 4 jets, 1 lepton and E_T^{miss} in the final state by applying different selection criteria and cut values. Apart from the desire to reduce the background events, these criteria must also ensure that the quality of the selected events are high, physics objects are well determined. In this regard, event selection process is applied at two different stages: Event preselection and final event selection. In this chapter, basic event selection criteria and the reconstruction strategies for the $Q\bar{Q}$ pair are explained. Obtained results after preselection are discussed in order to perform final event selection.

6.1. Event Preselection

Event preselection, can also be seen and called as 'the loose analysis'. For this part, the idea is to see the kinematic distributions both for the simulated samples and data. By looking into the comparison between data and MC, it is possible to implement necessary corrections if there is a need. Moreover, results taken in the preselection stage may provide necessary motivations for further cuts. Event preselection has both the analysis specific requirements such as having the final state objects in an event and also the independent criteria depending on the detector conditions. All the requirements and selection criteria are described separately.

6.1.1. Data Quality Cuts

As mentioned in the Section 5.1, ATLAS detector has collected data in different periods of LHC activity. Since the conditions of the runs may differ due to the unexpected things, it is possible to talk about the quality of runs. To eliminate the unreliable data, low quality events are removed from the data as given below.

Table 6.1. Event preselection cut list.

Cut Number	Cut List
Cut 1	All weighted events
Cut 2	GRL
Cut 3	Tile Error
Cut 4	LarErr
Cut 5	Tile Trip
Cut 6	Trigger
Cut 7	Number of Vertex Tracks>=5
Cut 8	Number of jets>0
Cut 9	At least 1 lepton
Cut 10	Exactly 1 e/m $P_T > 25/25$
Cut 11	Electron or Muon
Cut 12	Trigger match
Cut 13	e-mu overlap
Cut 14	bad goodJets>0
Cut 15	E_T^{miss} (m/e)>20/30
Cut 16	m_W^T (m/e)>60/30 GeV
Cut 17	Heavy Flavor
Cut 18	Flavor flag is 3
Cut 19	Leading jet P_T> 60
Cut 20	Number of good jets< 4

- Quality information is defined for the luminosity blocks (LB) of data which roughly corresponds to two minutes time of data taking. LBs considered as qualified enough, are recorded in the Good-Runs-Lists (GRLs), maintained by the Data Quality (DQ) group of ATLAS. If an event does not belong to a LB in the GRL, it is removed. Depending on the subdetectors involved, different analyses utilize somewhat different GRLs. The GRL used in this analysis is the one recommended for top quark measurements [1] (Cut 2).

[1] `data12_8TeV.periodAllYear_DetStatus-v61-pro14-02_DQDefects-00-01-00_PHYS_StandardGRL_All_Good.xml`

- Events with the *TileCal* and *TileTrip* error flags are rejected. These flags are related to the problems in Tile calorimeter. For instance, *TileCal* errors are present in those events taken when some Tile calorimeter cells are overheated (Cut 3 & Cut 5).
- Events with the *LAr* error flag are removed. This flag is given to the events due to the problems in Liquid Argon Calorimeter (Cut 4).

6.1.2. Object and Event Quality Cuts

Object quality cuts are the requirements on the physics objects.

- A quality cut is applied to the first primary vertex candidate in the PV candidate vertex container (VxPrimaryCandidate). The candidate should have at least 5 tracks and its type should be either PV or a pile up vertex (Cut 7).
- An overlap removal is done between electron and muon since muons can also be misidentified as electrons in ID (Cut 13).
- Quality of the jets are revisited by ATLAS JetEtmiss group after the reconstruction and low quality jets are labeled as 'bad'. If there is at least bad jet in an event, this event is eliminated (Cut 14).

6.1.3. Trigger Requirement

To decrease the number of background events it is possible to require the presence of a specific trigger signature in the event selection (Cut 6). Since the searched for events have a single lepton in the final state, either muon or electron triggers are required.

- For muons, events should have fired either `EF_mu24i_tight` or `EF_mu36_tight`.
- For electrons, events should have fired either `EF_e24vhi_medium1` or `EF_e60_medium1`.

The features of the desired trigger signatures can be recognized simply by looking at the naming conventions. EF means that the trigger chain is concluded at the EF, the

numbers are P_T thresholds for the specified lepton and final part refers to the quality of the relevant physics object [7].

6.1.4. Physics Objects Requirements and Kinematic Selection Criteria

The last part of the preselection is the set of 'loose' cuts to identify and reconstruct basic components needed in the analysis:

- Events are removed if there is no jet in the event (Cut 8).
- Events are removed if there is no lepton in the event (Cut 9).
- Exactly one lepton of $P_T > 25$ GeV should be present in the event (Cut 10).
- That lepton should be either an electron or an muon (Cut 11).
- E_T^{miss} should be higher than 20 GeV for muon channel and 30 GeV for electron channel (Cut 15).
- Transverse mass of the reconstructed W boson is defined as:

$$m_W^T = \sqrt{2P_T^l E_T^{miss}(1 - cos(\Delta\phi_{lv})} \tag{6.1}$$

  where $\Delta\phi_{lv}$ is the azimuthal (ϕ) angle between the lepton and the missing P_T (neutrino) and P_T^l is the lepton P_T. This variable is required to be higher than 60 GeV for events with muons and 30 GeV for events with electrons (Cut 16).
- Heavy Flavor overlap removal is done with a tool (HForTool) provided by ATLAS groups (Cut 17 & Cut 18).
- P_T of the leading jet (the highest P_T jet) should be greater than 60 GeV (Cut 19).
- Events are removed if the number of good jets in the event is less than 4 (Cut 20).

6.1.5. Control Regions

By requiring a different condition unlike the expectations of the studied channel, it is possible to study the final state in a signal free region. Having these kind of regions are useful to understand the modeling of the backgrounds and examine the agreement between data and simulation. Background and data comparisons, data driven corrections are also performed in these regions to provide a validation environment for the analysis.

In this analysis, to define extra control regions, preselection is loosened to allow events that have fewer than 4 jets. This way, three control regions are defined after cut 19. According to the number of jets in an event, the regions are labeled as 3 jets exclusive, 2 jets exclusive and 1 jet exclusive.

The agreement between data/MC are examined with the control plots, which can be seen in Appendix B.

6.2. Mass Reconstruction

After the event selection has been applied, mass reconstruction is performed in order to discriminate the heavy-quark decays from the background. Reconstruction of a particle is simply done by the addition of the four vectors of its decay products. The channel analyzed in this study, requires two stages of reconstruction. First two W bosons are reconstructed out of the final state objects. Then, using the reconstructed Ws and the associated jets, heavy quark reconstruction is carried out. Although the method seems quite straightforward, there are some important issues that must be resolved before the reconstruction, such as the estimation of the neutrino momentum and the correct association of jets and Ws.

6.2.1. Momentum Estimation for Neutrino

Leptonic W (W_{lep}) is reconstructed by combining the selected lepton and the neutrino information. However, direct reconstruction is not possible as the neutrinos escape the detector. The experimental results can only provide the E_T^{miss} information, therefore neutrino momentum in the z direction should be calculated or assumed somehow. It is possible to try to solve the two equations coming from the decay kinematics with two unknowns; assuming massless neutrinos and on-shell W bosons. If these equations do not yield real valued solutions for the neutrino energy, it is convenient to assume that the pseudorapidity of the neutrino is the same as that of the lepton since the W bosons are supposed to have large momentum if they are the daughters of a heavy quark. After completing the four vector definition of neutrino by this P_z estimation, W_{lep} can be reconstructed directly by adding the four vector of the lepton and the neutrino.

6.2.2. Jet Association

To be able to reconstruct the hadronic W mass ($m_{W_{had}}$), the correct combination of the 2 jets associated with the W_{had} must be chosen out of the 4 final state jets. Furthermore, the association of the remaining jets is also required for the reconstruction of the hadronic Q ($m_{Q_{had}}$) mass and the leptonic Q $m_{Q_{lep}}$ mass. Considering that $m_{W_{had}}$ should be close to the known nominal rest mass of the W boson, $M_W = 80.42$ GeV and the difference between the reconstructed $m_{Q_{had}}$ and $m_{Q_{lep}}$ is expected to be very small; a χ^2 minimization is applied to obtain the best scenarios for jet association. The definition of χ^2 can be found in Equation (6.2).

$$\chi^2 = \frac{m_{W_{had}} - M_W}{\sigma_W^2} + \frac{m_{Q_{had}} - m_{Q_{lep}}}{\sigma_{QQ}^2} \tag{6.2}$$

In the Equation (6.2), σ_W refers the width of the reconstructed W boson and it is optimized as 11 GeV (Figure 6.2.2); σ_{QQ} is the width of the reconstructed heavy quark

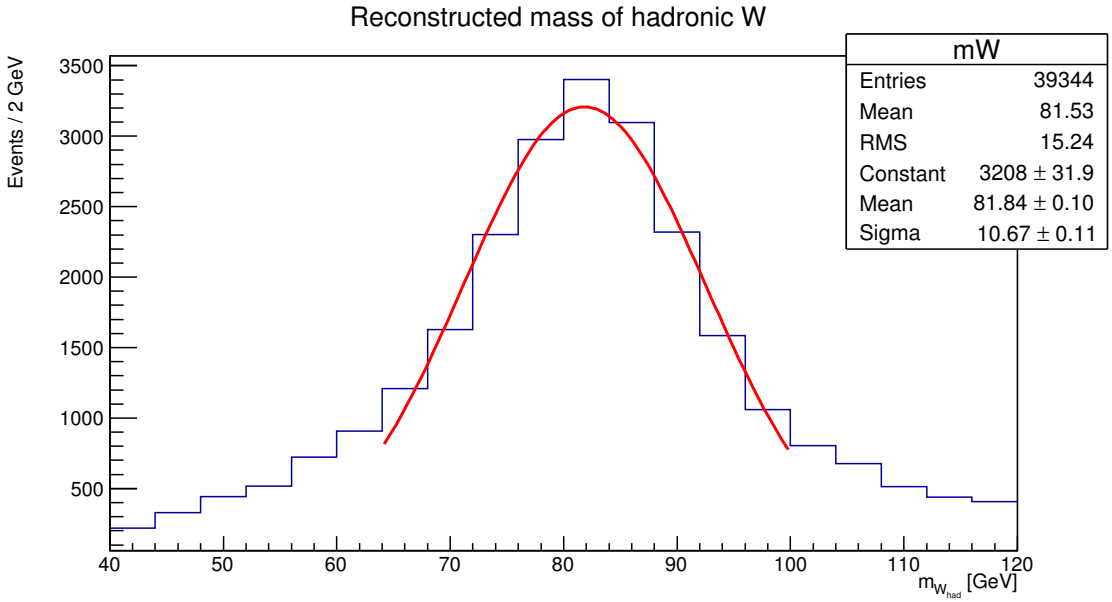

Figure 6.1. Reconstructed hadronic W mass in 500 GeV signal sample.

mass difference as determined for signal MC samples (Figure 6.2) and it is optimized as 35 GeV for 500 GeV t′ signal sample.

The jet combination with the minimum χ^2 is selected provided at least one of the heavy quarks is formed using either the leading or sub-leading jet. With this algorithm, jet association ambiguity is resolved and one heavy quark is reconstructed with the leptonically reconstructed W boson and the associated jet whereas the other heavy quark from the remaining three jets.

The reconstruction efficiency is computed as the ratio the number of events survived after all selection criteria to the all events in the sample. A histogram with each bin representing a cut is created, while keeping the first two bins for all events (with and without weights). Each other bin is filled with the weights of the events that pass all the cuts up to and including that bin. The reconstruction efficiency can hence be computed as the number of events in the last bin divided by the number of events in the second (ie. weighted total) bin. The weight for each event is obtained by: MC event weight × pileup weight × lepton efficiency weight × $\sum_{i=1}^{4} i^{th}$ jet efficiency weight. Here the object efficiency weights are each obtained from the tools of each respective performance group and they represent corrections addressing the small

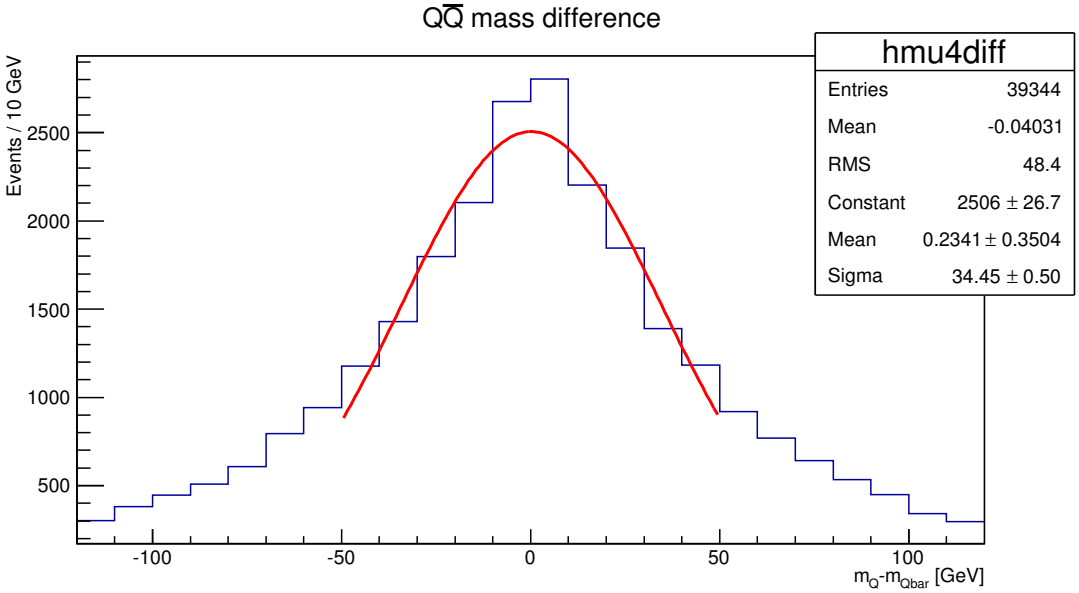

Figure 6.2. Mass difference of the reconstructed $Q\bar{Q}$ in 500 GeV signal sample.

differences between the observed object reconstruction efficiencies in data and MC.

6.3. Loose Analysis Results

After event preselection, it is necessary to evaluate the preliminary results in terms of a few aspects: level of agreement between data and MC, understanding the background modeling and motivating additional cuts for final selection in order to increase signal to background ratio.

Some of the kinematic distributions after preselection are presented in this section. In each plot, data is shown together with the simulated events where simulated events are normalized to the data luminosity of 20.3 fb^{-1}. The signal expectation for a t' mass of 500 GeV is also shown in the plots. The remaining distributions can be seen in the Appendix B .

By using Equation (5.2), charge asymmetry coefficients (CA) are calculated both for the electron and muon channels after Cut 19 (Section 6.1). The calculation is done just before requiring at least 4 jets in the final state events, since the coefficients are also computed for the control regions of the analysis. All of these coefficients can be

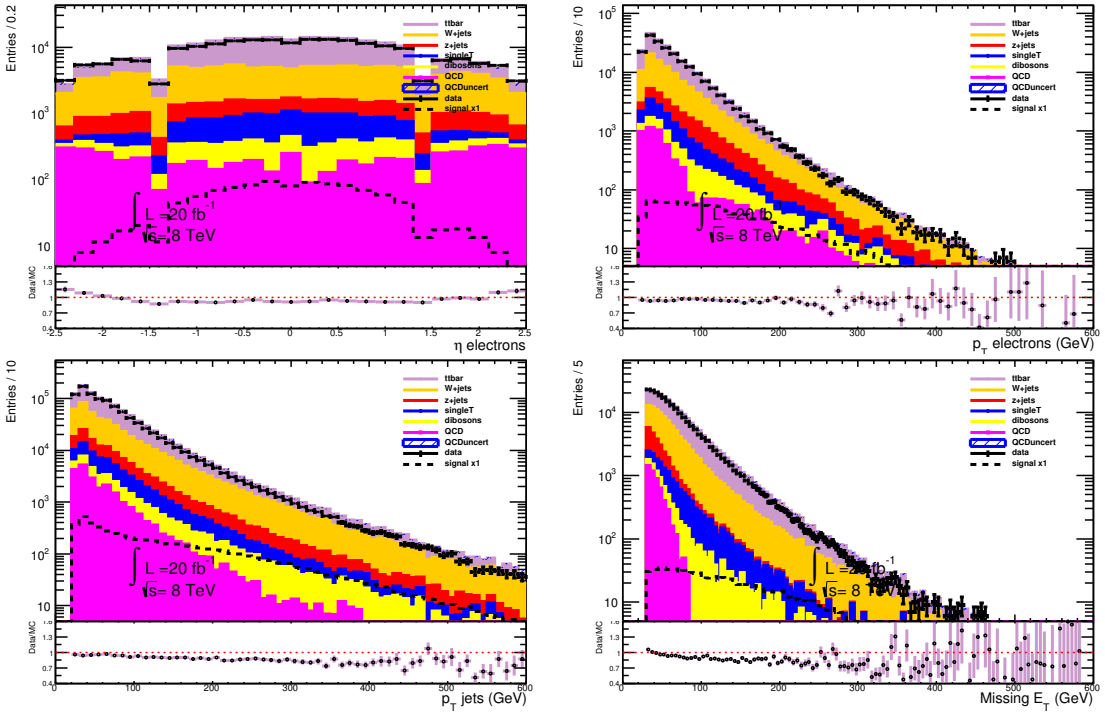

Figure 6.3. P_T and η of electrons, P_T of jets, E_T^{miss} distribution in electron channel.

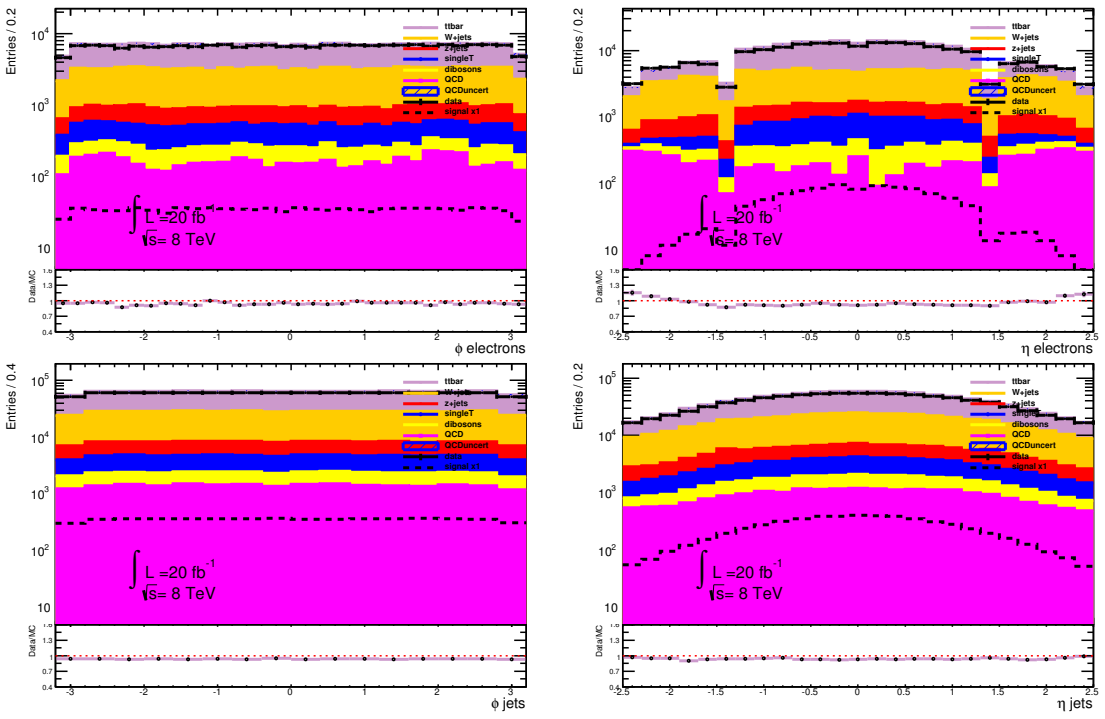

Figure 6.4. ϕ distributions of the objects, η distribution of the jets in electron channel.

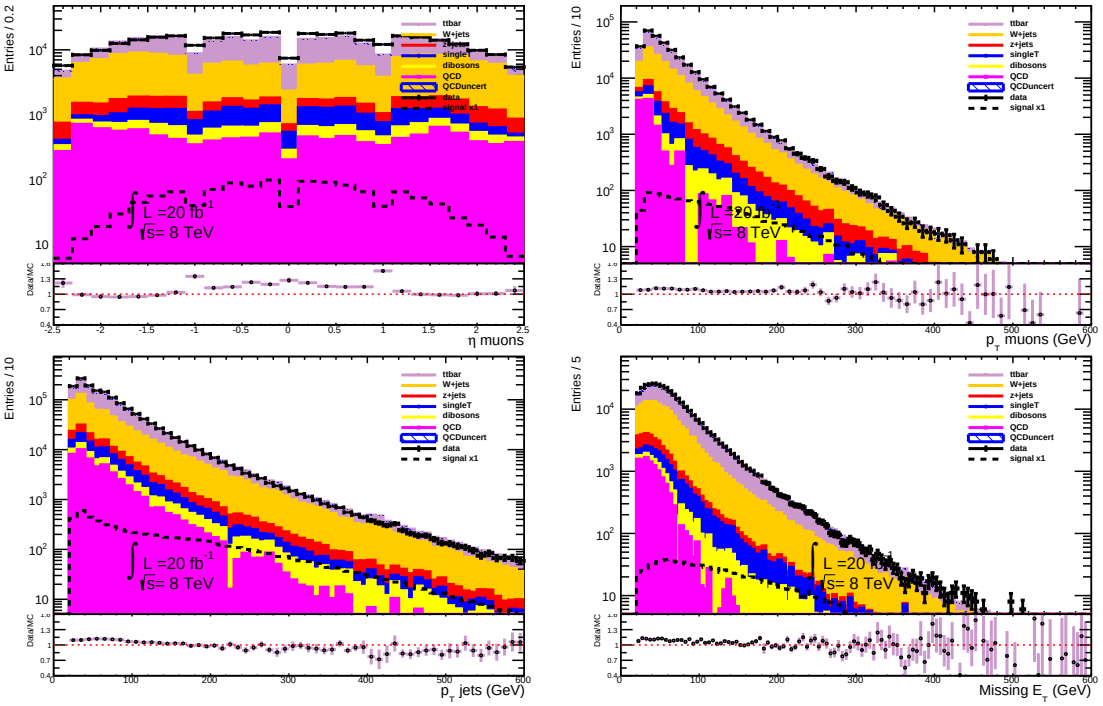

Figure 6.5. P_T and η of muons, P_T of jets, E_T^{miss} distribution in muon channel.

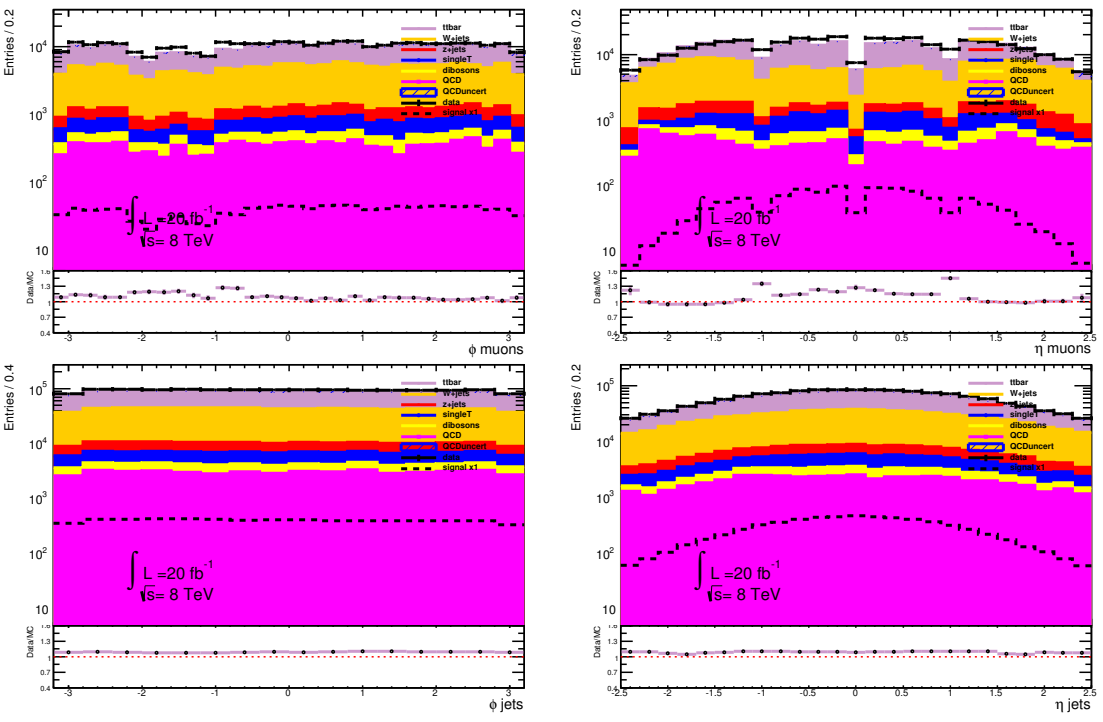

Figure 6.6. ϕ distributions of the objects, η distribution of the jets in muon channel.

Table 6.2. CA coefficients derived for different number of jets after loose analysis.

Number of Jets	CA for Electron Channel	CA for Muon Channel
1 jet exclusive	0.99	1.20
2 jets exclusive	1.04	1.29
3 jets exclusive	0.95	1.21
4 jets exclusive	0.85	1.02

found in Table 6.2.

Data/MC ratio can be investigated through Figure 6.4 for electrons and Figure 6.6 muons channels. The ratios are mostly around unity but from the η and ϕ distributions, it can be said that the normalization of the electron channel agrees slightly better than that of the muon channel.

By looking at the P_T distributions in Figure 6.3 and Figure 6.5, the remaining minor discrepancy in the P_T shape (Section 5.4.1) left from the applied W+jet correction can still be observed.

The yields of the loose analysis and selection efficiencies are summarized in Table 6.3 and Table 6.4.

Table 6.3. Preselection yields.

Sample	Electron	Muon
BG	2.39e+05	3.21e+05
$t\bar{t}$	1.22e+05	1.47e+05
W+jets (Sherpa)	7.94e+04	1.36e+05
W+jets (Alpgen)	7.199e+04	1.257e+05
Z+jets	2.04e+04	1.23e+04
Single Top	8475	9868
Dibosons	3497	4307
QCD	5638	1.21e+04
500 GeV signal	1217	1215

Table 6.4. $t\bar{t}$ sample cut flow in electron channel with loose cuts.

Requirement	Cut List	# Events Passed	Cut Efficiency
Cut 1	All weighted events	14930068	$0.9956 \pm 1.701\times10^{-5}$
Cut 2	GRL	14930068	1 ± 0
Cut 3	Tile Error	14930068	1 ± 0
Cut 4	Lar Error	14930068	1 ± 0
Cut 5	Tile Trip	14930068	1 ± 0
Cut 6	Trigger	3770240	$0.2525 \pm 1.124\times10^{-4}$
Cut 7	Number of vertex tracks ≥ 5	3768806.25	$0.9996 \pm 1.004\times10^{-5}$
Cut 8	Number of jets> 0	3748127.5	$0.9945 \pm 3.805\times10^{-5}$
Cut 9	At least 1 lepton	2468951.25	$0.6587 \pm 2.449 \times10^{-4}$
Cut 10	Exactly 1 e/m $P_T > 25/25$	2404174.5	$0.9738 \pm 1.017 \times10^{-4}$
Cut 11	Electron or Muon	2221666.75	$0.9241 \pm 1.708 \times10^{-4}$
Cut 12	Trigger match	2219830.5	$0.9992 \pm 1.928 \times10^{-5}$
Cut 13	e-mu overlap	2219517.5	$0.9999 \pm 7.969 \times10^{-6}$
Cut 14	Bad goodJets > 0	2216239.25	$0.9985 \pm 2.578\times10^{-5}$
Cut 15	E_T^{miss} (m/e) $> 20/30$ GeV	1781785.625	$0.804 \pm 2.667 \times10^{-4}$
Cut 16	m_W^T (m/e) $> 60/30$ GeV	1533370.625	$0.8606\pm 2.595 \times10^{-4}$
Cut 17	Heavy Flavor	1493470.5	$0.974 \pm 1.286 \times10^{-4}$
Cut 18	Flavor flag is 3	1493470.5	1 ± 0
Cut 19	Leading jet $P_T> 60$	1282203	$0.8585 \pm 2.852\times10^{-4}$
Cut 20	Number of good jets < 4	652388.0625	$0.5088 \pm4.415\times10^{-4}$

7. SYSTEMATIC UNCERTAINTIES

There are various systematic uncertainties on the measured observables and all of them needs to be propagated to the final distributions of the discriminant. Limit setting can only be done after considering all these systematic effects.

To be able to interpret any excess in the data as a signal, the effect of the systematic uncertainties on final discriminant should be understood well. For this analysis, the systematic uncertainties are mainly caused by the measurements of the final state objects, bad modeling of the main backgrounds. The uncertainty of each error source is either derived for this channel by running the analysis for that specific variable or taken from the results, which are based on various studies, suggested by ATLAS performance groups.

Table 7.1. Summary of energy smearing and scaling for physics objects.

Objects	E_T Scaling	E_T Sc. syst	E_T Smearing	E_T Sm. syst
Electrons	Data	MC	MC	MC
Muons	MC	MC	MC	MC
Jets:JES	MC and Data	MC or Data	No	No
Jets:JER	No	No	No	MC
Jets:JVF	MC	MC	N/A	N/A
MET	Data(e) and MC(m,j)	MC	MC	MC

7.1. Luminosity

Uncertainty on the total integrated luminosity is given as ±2.8% by ATLAS Luminosity group.

7.2. Physic Objects Uncertainties

7.2.1. Jet Energy Scale

One of the significant error sources for the jets is the uncertainties related with the jet energy scaling (JES). Since the tasks and algorithms for jets are most challenging and complicated ones, many parameters contribute to the total uncertainty calculation for the jet features.

There are various configurations for handling JES uncertainties. In this analysis one of the possible configurations[2] is chosen which includes 20 parameters. 12 of them are in-situ nuisance parameters sorted into 5 categories:

(i) Statistical: statistical and method uncertainties.
(ii) Detector: detector uncertainties.
(iii) Modelling: modelling/theory uncertainties.
(iv) Mixed: mixed detector and modelling uncertainties.
(v) Special: a few select parameters, such as pile-up terms.

The remaining 8 parameters are based on the η intercalibration, pile-up high P_T and closure issues. All of these parameters should be evaluated with the flavor and topology uncertainties of the objects in detectors[3] .

7.2.2. Jet Energy Resolution

The uncertainty coming from the jet energy resolution (JER) is needed to be taken into account. To evaluate the JER systematic each jet has been scaled with a random factor that belongs to a Gaussian distribution whose mean value is 1 and the σ value is the smearing factor. That smearing factor has been calculated from the quadrature difference between the truth resolution of the jet plus its uncertainty

[2]InsituJES2012_20NP_ByCategory.config
[3]MultijetJES_2012.config

and the truth resolution. The truth resolution for a jet and its uncertainty has been obtained by using the tool[4] provided by the ATLAS JetEtmiss group. The uncertainty for the JER is symmetric; therefore up and down variations are considered to yield the same level of variation in the final results.

7.2.3. Jet Reconstruction Efficiency

Depending on the P_T and η values of the jets, some of them are removed from the event randomly. The analysis is done with the remaining jets, which can be considered as relatively good jets. The uncertainty calculated with this method is symmetrised and used both for the plus and minus variations in the final results.

7.2.4. Muon Momentum Scale and Resolution

Systematic uncertainty for muon momentum smearing and resolution are separately calculated for MS and ID since the estimation of muon momentum depends on both of these detector components. For these variations, additional runs are done. For the MS, mptsmear0 and mptsmear1 are up and down variations and for the ID mptsmear2 and mptsmear3 are up and down versions. Uncertainty for the muon P_T scale offset is also considered with separate runs and the corresponding variables are labeled as mptsmear4 and mptsmear5 respectively for up and down variations. In Figure 7.1, the variations for MS component is illustrated, mptsmear0 and mptsmear1.

7.2.5. Muon top-Id efficiency SF

The uncertainty on the isolation cuts is determined as $\pm 0.5\%$ per muon.

[4]JERProvider used with JERProviderPlots_2012.root

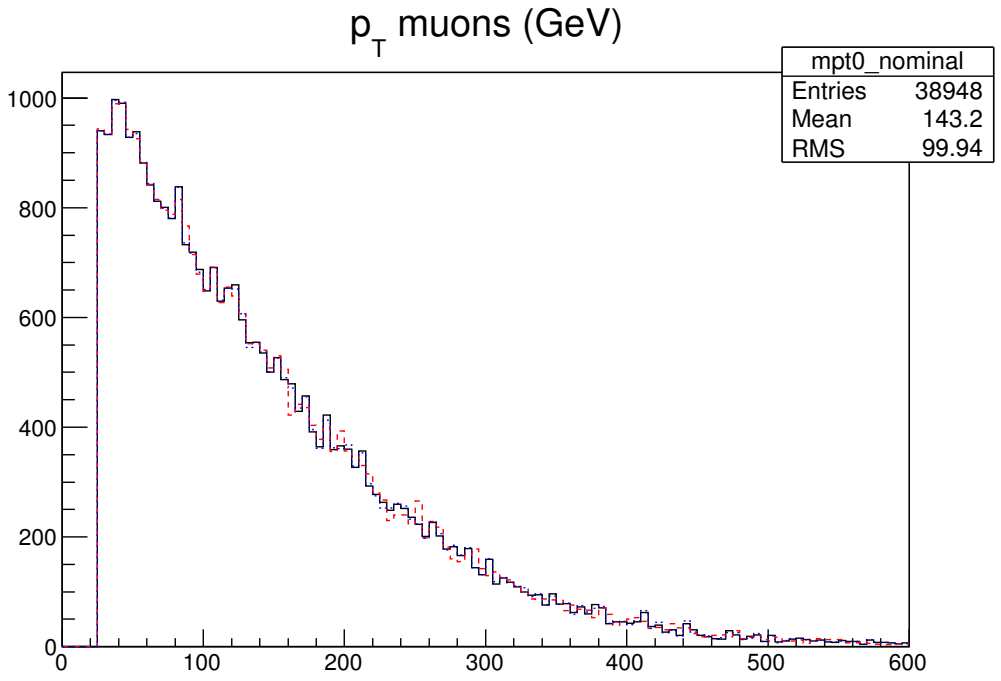

Figure 7.1. The effect of the ± 1 σ variations of MS muon momentum smearing on muon P_T distribution of 600 GeV signal sample.

7.2.6. Electron Energy Scale and Resolution

A package[5] written by the egamma group (the performance group that studies electron and photon objects in ATLAS) is used in order to calculate the uncertainties.

7.2.7. Electron Reconstruction, ID efficiency and Isolation Factors

Reconstruction, trigger and ID efficiencies for electrons have been extracted from a tool[6] . The tool requires the relevant run number, P_T and cluster η information for each electron. Each uncertainty is calculated by varying the relevant scale factors: esfrc0 and esfrc1 are for reconstruction efficiency; esfid0 and esfid1 are up and down variations for the ID; esftr0 and esftr1 refer to the uncertainties trigger.

[5]EnergyRescalerUpgrade
[6]Electron Efficiency Correction

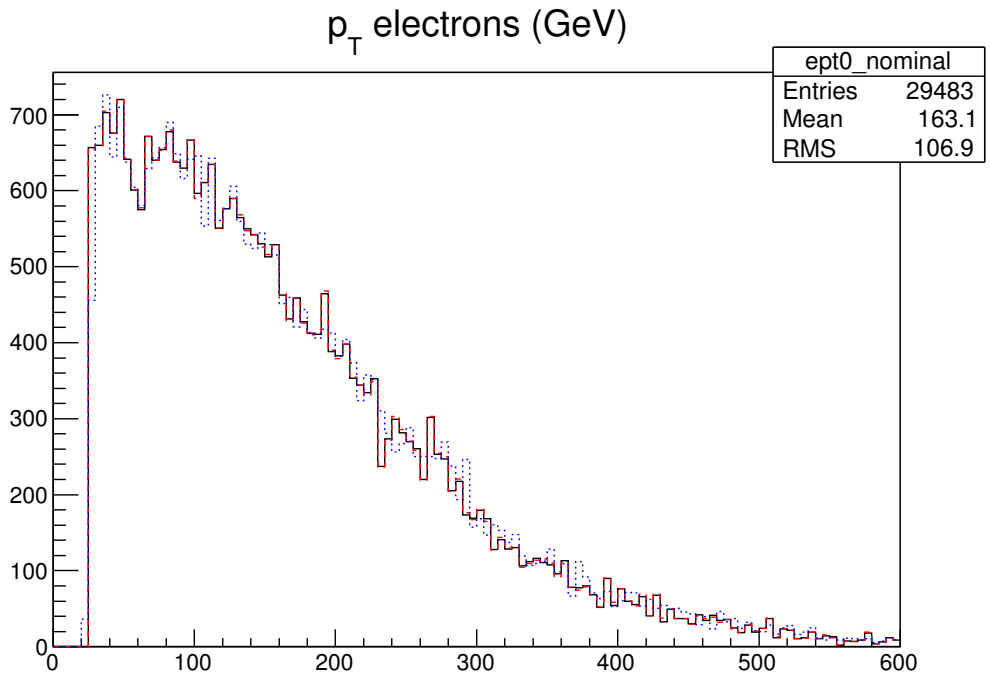

Figure 7.2. The effect of the $\pm 1\sigma$ variations of electron energy smearing on electron P_T distribution of 600 GeV signal sample.

7.3. Systematic Uncertainty for W+jets Background

In Section 5.4.1, the derivation of the CA coefficient is given. Propagating the uncertainty on N_{W^+} and N_{W^-} variables, standard deviation of the normalization factors are found. The uncertainties for both the electron and the muon channel are given in Table 7.2.

Table 7.2. Standard Deviations for CA normalization factors.

	electron		muon	
	CA	σ_{CA}	CA	σ_{CA}
4 jet	0.850	± 0.0899	0.938	± 0.120
3 jet	0.951	± 0.0660	1.161	$\pm$ 0.101
2 jet	1.041	± 0.048	1.238	$\pm$ 0.067
1 jet	0.989	± 0.0324	1.156	± 0.043

Table 7.3. Systematic uncertainties for leptons, calculated after final selection, uncertainties are given in % both for electron channel and muon channel separately.

	electron			muon	
Systematic type	W+jets	$t\bar{t}$ sample	500 GeV signal	$t\bar{t}$ sample	500 GeV signal
mptsmear0/1	0.007/0.002	0.00/0.00	0.03/0.001	0.067/0.082	0.053/0.134
mptsmear2/3	0.002/0.003	-0.009/-0.008	0.001/0.013	0.087/0.070	0.070/0.129
mptsmear4/5	0.001/0.005	-0.008/0.001	0.001/0.018	0.148/0.009	0.041/0.114
escaler0/1	0.001/0.304	0.048/0.141	0.225/0.528	-0.007/0.001	-0.002/0
mutrig0/1	0/0	0/0	0/0	1.242/-1.065	1.251/-1.069
esfrc0/1	2.497/1.704	2.7334/2.117	2.455/1.633	0/0	0/0
esfid0/1	1.905/-0.070	1.481/-0.121	1.75403/-0.200	0/0	0/0
esftr0/1	1.865/0.931	2.28282/1.51	1.889/1.106	0/0	0/0

Table 7.4. Jet uncertainties calculated after final selection, uncertainties are given in % both for electron channel and muon channel separately.

	electron			muon	
Systematic type	W+jets	$t\bar{t}$ sample	500 GeV signal	$t\bar{t}$ sample	500 GeV signal
JER	1.04/1.04	+3.56/-3.56	+0.99/-0.99	+0.66/-0.66	-5.12/+5.12
jetreco	-0.03/0.03	-0.01	-0.00	0.01	-0.01
jescomU0/1	0.757444/-0.213	0.470/-0.093	0.090/0.009	0.322/-0.072	0.135/-0.013
jescomU10/11	-0.001/0.258	0.035/0.158	0.001/-0.008	0.030/0.070	-0.025/0.024
jescomU12/13	3.00211/0.873	2.883/0.856	0.152/0.023	2.945/0.732	0.414/0.167
jescomU14/15	0	0/0	0/0	0/0	0/0
jescomU2/3	0.471/4.877	0.588/3.908	0.008/0.892	0.426/3.574	0.076/0.889
jescomU4/5	-0.034288/-0.037	0.531/-0.180	-0.064/0.002	0.639/-0.208	-0.085/-0.031
jescomU6/7	0.200/1.721	0.327/2.193	-0.034/0.117	0.279/2.036	0.015/0.334
jescomU8/9	-0.114/0.241	-0.259/0.306	0.027/-0.010	-0.266/0.247	-0.040/0.031
jescomD0/1	-0.834/0.180	-0.411/0.097	-0.063/0.016	-0.290/0.064	-0.124/-0.004
jescomD10/11	-0.012/-0.323	-0.057/-0.159	-0.030/-0.004	-0.022/-0.086	0.006/-0.047
jescomD12/13	-3.072/-0.999	-2.847/-0.747	-0.353/-0.009	-2.693/-0.651	-0.440/-0.099
jescomD14/15	0/0	0/0	0/0	0/0	0/0
jescomD2/3	-0.551/-4.930	-0.456/-3.687	0.007/-0.760	-0.399/-3.358	-0.123/-0.861
jescomD4/5	-0.008/-0.024	-0.514/0.226	0.264/-0.053	-0.580/0.241	0.015/-0.012
jescomD6/7	-0.212/-1.794	-0.284/-2.154	-0.021/0.036	-0.259/-1.960	-0.067/-0.226
jescomD8/9	0.033/-0.264	0.295/-0.260	-0.036/-0.024	0.293/-0.180	-0.002/-0.028

8. FINAL EVENT SELECTION AND LIMIT SETTING

To be able to increase the signal to background ratio, tighter cuts are applied on top of the preselection criteria. Discriminant variables are obtained after tight analysis separately for electron and muon channels. Considering the systematic uncertainties discussed in Section 7, limit setting is performed using the reconstructed Q mass as the discriminant in the pretag condition. In pretag condition, without requiring any flavor criteria for final state jets, both the b-tagged jets and the light jets are accepted. This chapter presents the tight cuts applied for the final event selection, discriminants used for limit setting and finally the observed limit of this analysis.

8.1. Tight Cuts

All of the tight cuts are motivated by the kinematic distributions obtained after event preselection. Corresponding P_T distributions have been already presented in Figures 6.3 and 6.5 both for the electron and muon channel. Additional distributions can be seen in Figure 8.1 and Figure 8.2.

- ΔR between the reconstructed Q_{lep} and Q_{had} 4 momenta should be higher than 2 and less than 4.1 mm,
  $2 < \Delta R(Q_{lep}, Q_{had}) < 4.1$.
- Cosine of the angle between two jets forming the W_{had} should be higher than 0.
- Mass difference between Q_{lep} and Q_{had} should be less than 150 GeV,
  $\Delta(M_{Q_{lep}}, M_{Q_{had}}) < 150$ GeV.
- P_T of the leading jet should be higher than 150 GeV.
- P_T of the second leading jet should be higher than 60 GeV.
- An optional cut for b-jet identifications, meaning that requiring at least one b-jet(1b) in the events or removing the events with b-jets (b-veto case, 0b) is possible.

Final selection yields and efficiencies can be seen in Table 8.1 and 8.2.

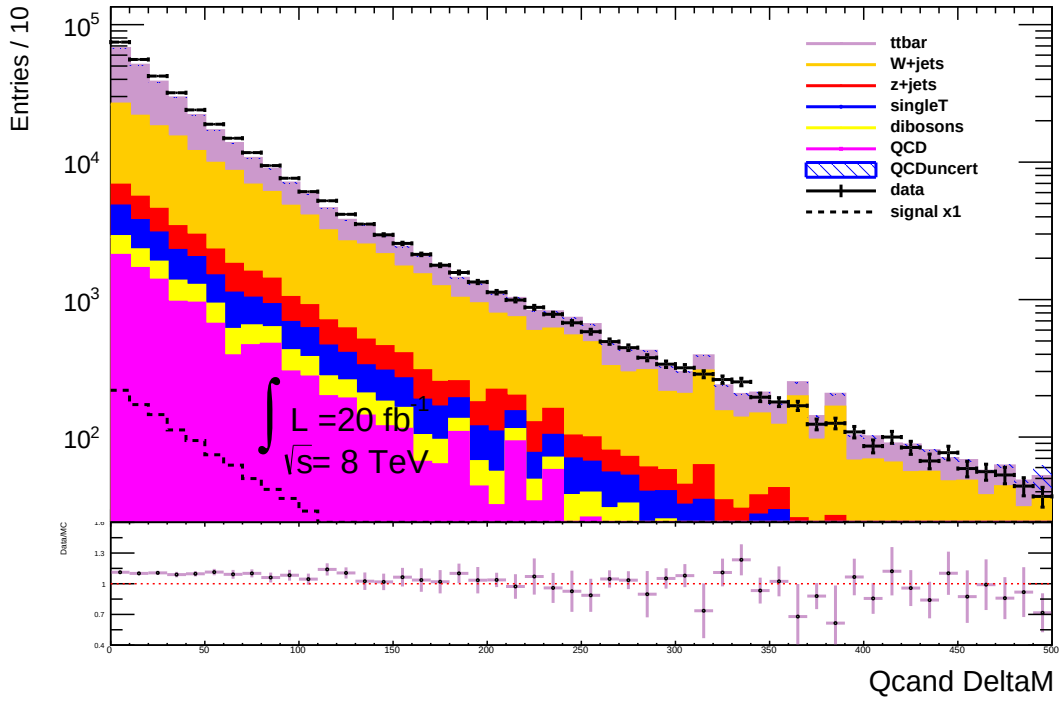

Figure 8.1. Difference between $M_{Q_{lep}}$ and $M_{Q_{had}}$ after preselection in muon channel.

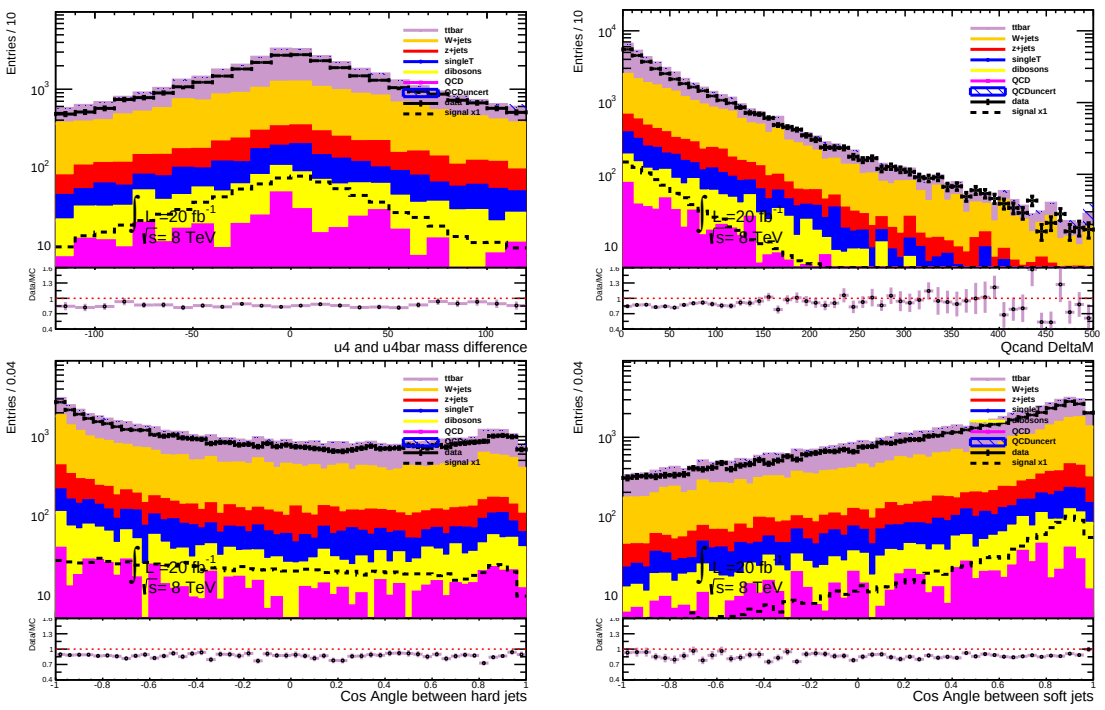

Figure 8.2. Top plots show the mass difference between reconstructed new quarks, left bottom plot is the cosine of the angle between two jets coming from the Q quarks, right bottom plot is cosine of the angle between two jets forming the W_{had} after preselection in electron channel.

Table 8.1. Final selection yields.

Sample	Electron	Muon
BG	32041.8	42050.3
$t\bar{t}$	16898.41	20458.1
W+jets	11171	16946.44
Z+jets	1863.2	1755.23
Single t	1067.66	1225.76
Dibosons	727.315	898.748
QCD	331.745	790.791
300 GeV signal	12176	13831.9
400 GeV signal	2707	3018.73
500 GeV signal	728.972	819.168
600 GeV signal	235.193	245.271
700 GeV signal	79.2157	79.266
800 GeV signal	26.377	27.1396
Data	27572	42341

After applying tight cuts, the comparison between data and MC has been revisited. Remaining kinematic distributions produced with tight analysis are given in Appendix . Investigating these results shows that the ratio of the data/MC is still around unity, however a minor normalization issue is observed in the electron channel unlike the preselection results.

The observed normalization issue both in the preselection and the final selection results are covered by the systematic uncertainties, particularly within the uncertainty in the σ_{CA} correction factor that is applied to the normalization. To resolve the normalization issue in the electron channel, initially the mass distribution below 350 GeV is unblinded and a final scaling factor for the electron channel is determined using the unblinded result (Figure 8.3). Proceeding to the limit setting has shown that results don't change significantly whether this final scaling is applied or not. Therefore, applying an additional scaling for electron channel, normalized distributions are used to

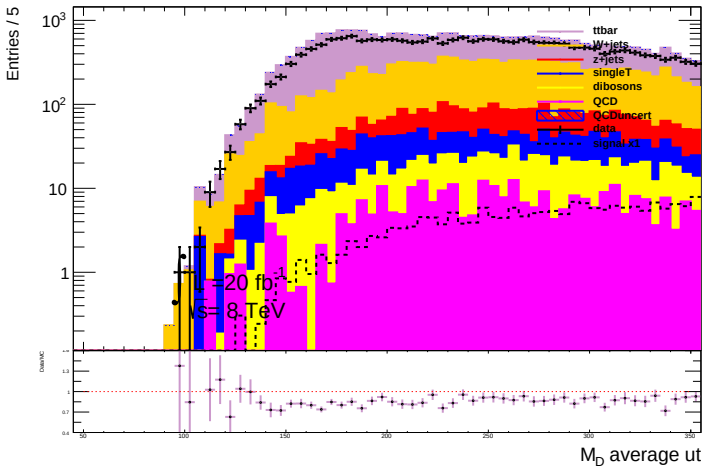

Figure 8.3. Partial unblinding in electron channel, the average value of $m_{Q_{had}}$ and $m_{Q_{lep}}$ up to 350 GeV.

obtain presented results.

Although this normalization factor can be covered by the calculated uncertainties, understanding the reason behind the change between the loose and tight analysis is important. In order to do that, additional runs have been done separately by changing the each cut separately to see the effect of the individual cuts. From these investigations, it is understood that, the simulation overestimates the number of W+jets events compared to the data-driven determination by up to 15%, depending on the jet multiplicity.

8.2. Limit Setting

As the final discriminant for this analysis, invariant mass of the Q is used. After the determination of $m_{Q_{lep}}$ and $m_{Q_{had}}$, invariant mass of Q (m_Q) is calculated by taking their average. Figure 8.4 shows the distribution of m_Q after final selection separately for electron and muon channels.

Limit setting is done using the software MClimit [24]. The tool uses the CLs method [25] and the limit is calculated with the frequentist approach. A log-likelihood method is utilized to examine the data under the background and signal+background

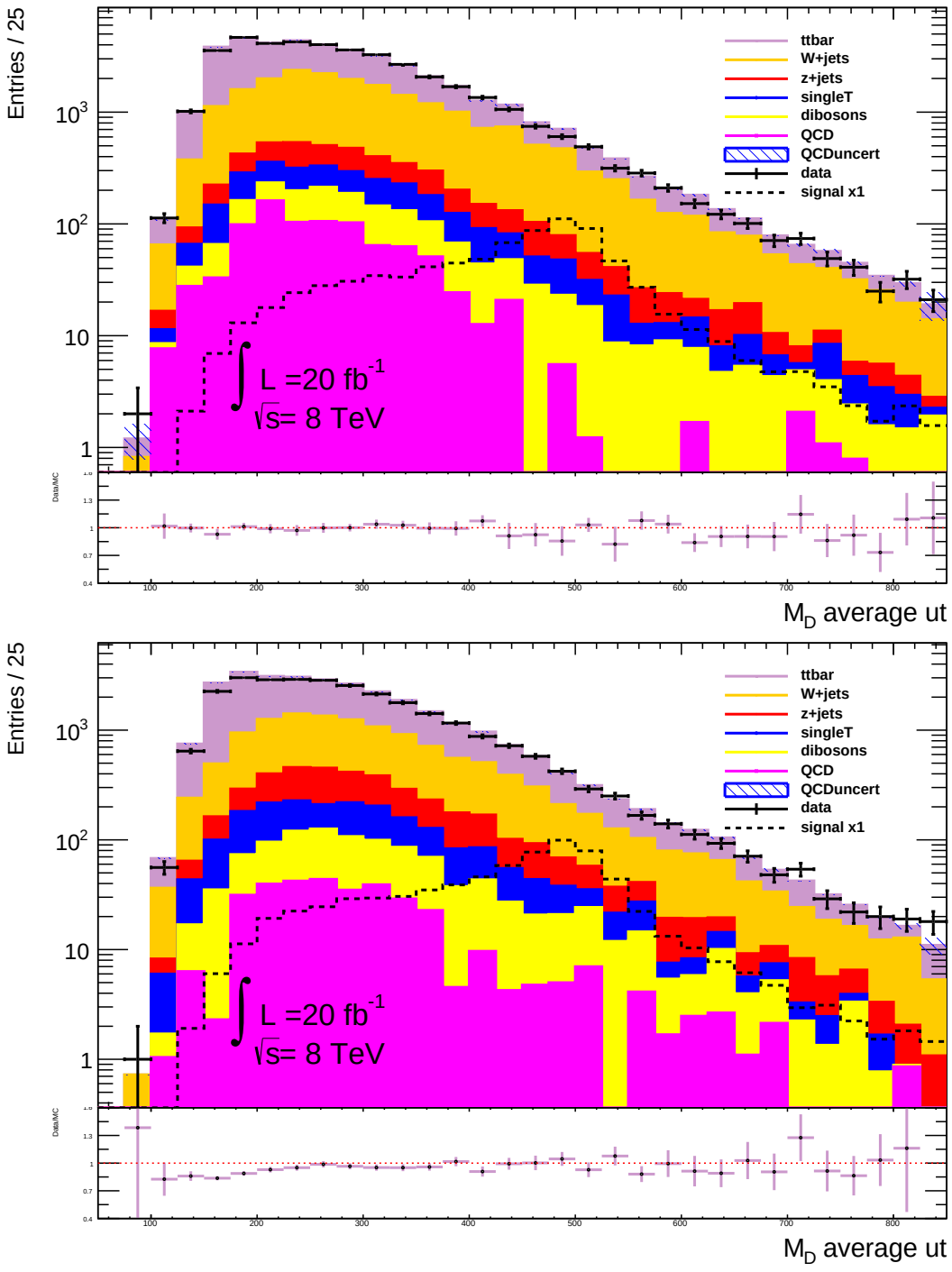

Figure 8.4. Average invariant mass of Q in muon (top) and electron (bottom) channels.

hypotheses to put a limit on the presence of the proposed quark.

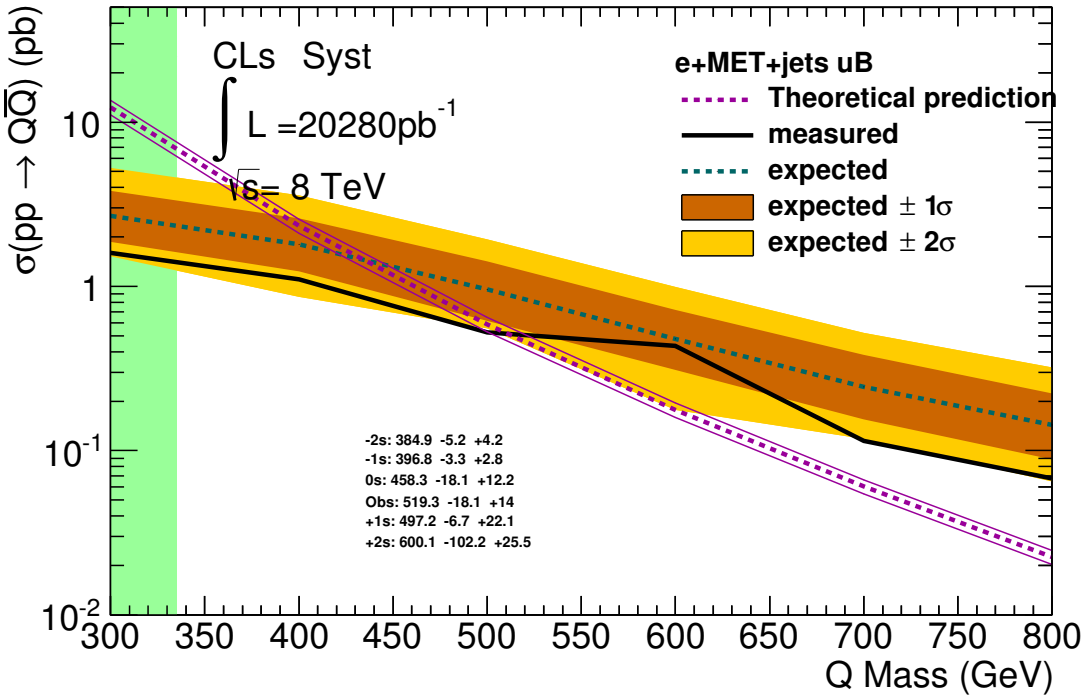

Figure 8.5. Limit with 95% confidence level for electron channel only.

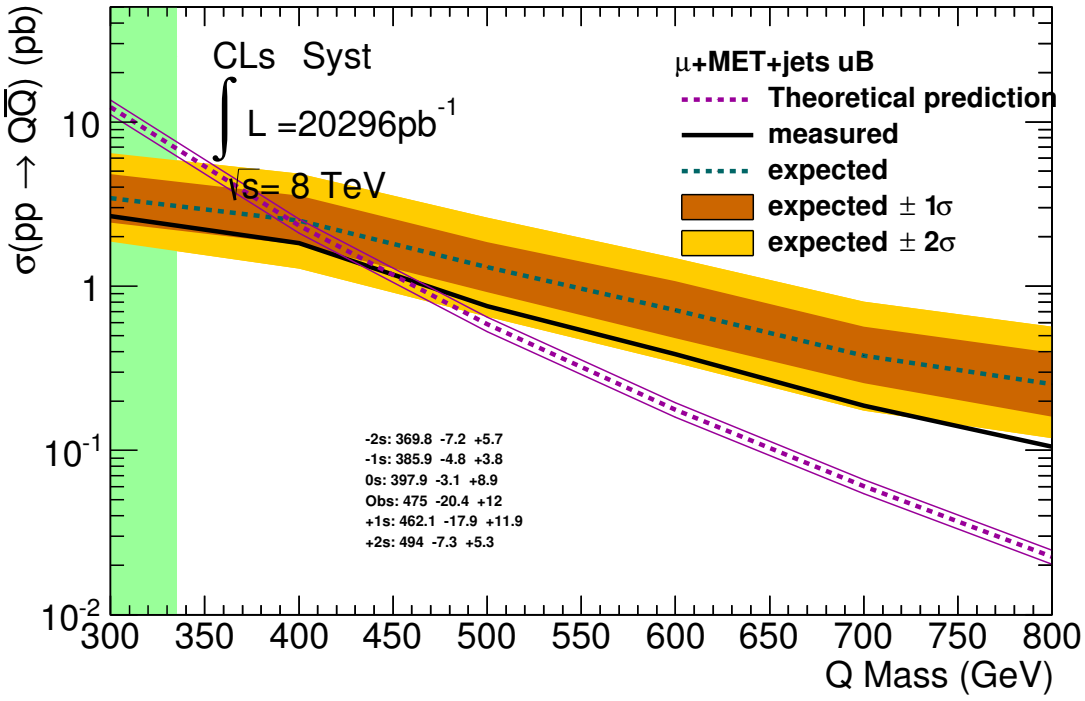

Figure 8.6. Limit with 95% confidence level for muon channel only.

8.3. Final Selection with Light quarks:B-veto

As it is mentioned in the Section 8.1, as an additional cut, b-tagging can be used for event selection. Either the events are required with at least 1 b-jet (1b scenario) or they can be rejected if they have one or more b-jets (b-veto case, 0b scenario). From the theoretical point of view, both scenarios can be foreseen as equally interesting BSM scenarios. Since the 1b jet scenario has been investigated recently in ATLAS, b-veto case is a fresh and complementary study.

To be able to extract a limit for a signature, one has to use a signal sample produced exactly for the desired process. However, the signal samples used in this study are mixed samples (Section 5.2). Hence, they are not appropriate for studying b-jet scenarios until they are separated into two groups: with and without b-jet. It is possible to perform this task by doing truth matching for each of the mass points of the signal samples, but due to technical difficulties, the detailed analyses is leaved for a future study. What is done in this section is just to provide an idea for such future studies and conforming the pretag results by providing additional material for investigation.

The production information of the signal samples are evaluated and then a generic estimation is done for the total number of events that have b-jets and light jets. Using the branching fraction information and the efficiency of the b-tagging mechanism in ATLAS, a ratio is obtained for the subgroups of the signal samples. By using this ratio as a scale factor for the signal samples, limit setting is done also for b-veto case and the result can be seen in Figure 8.7.

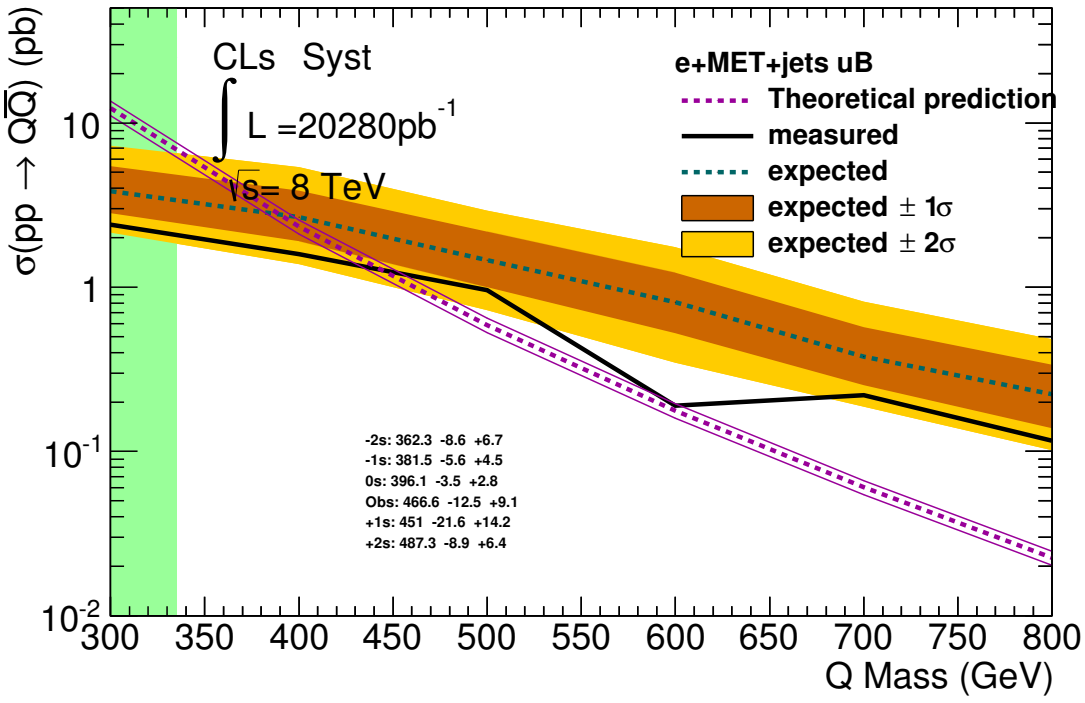

Figure 8.7. Obtained Limit for b-veto case with 95% confidence level for electron channel only.

Table 8.2. $t\bar{t}$ sample cut flow in electron channel with tight cuts.

Requirement	Number of Events Passed	Cut Efficiency
All weighted events	14930068	0.9956± 1.701 $\times 10^{-5}$
GRL	14930068	1 ± 0
Tile Error	14930068	1 ± 0
LarErr	14930068	1 ± 0
Tile Trip	14930068	1 ± 0
Trigger	3770240	0.2525 ± 1.124$\times 10^{-4}$
Number of Vertex Tracks$\geq$5	3768806.25	0.9996 ± 1.004$\times 10^{-5}$
Number of jets>0	3748127.5	0.9945 ± 3.805$\times 10^{-5}$
At least 1 lepton	2468951.25	0.6587 ± 2.449$\times 10^{-4}$
Exactly 1 e/m $P_T > 25/25$	2404174.5	0.9738 ± 1.017$\times 10^{-4}$
e OR m	2221666.75	0.9241 ± 1.708$\times 10^{-4}$
Trigger match	2219830.5	0.9992 ± 1.928$\times 10^{-5}$
e-mu overlap	2219517.5	0.9999 ± 7.969$\times 10^{-6}$
bad goodJets>0	2216239.25	0.9985 ± 2.578$\times 10^{-5}$
E_T^{miss} (m/e)>20/30	1781785.625	0.804 ± 2.667$\times 10^{-4}$
m_W^T (m/e)>60/30 GeV	1533370.625	0.8606 ± 2.595$\times 10^{-4}$
Heavy Flavor	1493470.5	0.974 ± 1.286$\times 10^{-4}$
Flavor flag is 3	1493470.5	1 ± 0
Leading jet P_T>60	1282203	0.8585 ± 2.852$\times 10^{-4}$
Number of good jets¡4	652388.0625	0.5088 ± 4.415$\times 10^{-5}$
2nd leading jet P_T>60	478067.375	0.7328 ± 5.478$\times 10^{-4}$
ϕ(met,j0)>0.2	478067.375	1 ± 0
Leading jetP_T>150	147790.9688	0.3091 ± 6.684$\times 10^{-4}$
Cos angle soft jets>0	112099.7422	0.7585 ± 1.113$\times 10^{-3}$
$\Delta(M_{Q_{lep}}, M_{Q_{had}}) < 150$	100638.3984	0.8978 ± 9.049$\times 10^{-4}$
$2 < \Delta R(Q_{lep}, Q_{had}) < 4.1$	90595.8125	0.9002 ± 9.448$\times 10^{-4}$
Number of b-tagged $\geq$1 jet	80594.03125	0.8896 ± 1.041$\times 10^{-3}$

9. CONCLUSIONS

In this study, a possible scenario for the pair produced heavy quarks at the LHC has been analyzed by assuming that the new quarks decay via the W boson channel. The search is considered as a signature based generic study, since it is applicable for different models.

Quarks masses below 519 GeV has been excluded at the 95% confidence level in electron channel and 475 GeV in muon channel, while the expected limit based on MC studies is 458 GeV and 398 GeV respectively. For the b-veto scenario, the expected and observed limits are found to be weaker (around 466 GeV observed limit at 95%CL), indicating for future studies the need for dedicated cut optimization before the application of b-jet-related requirements.

APPENDIX A: PLOTS FOR FINAL SELECTIONS

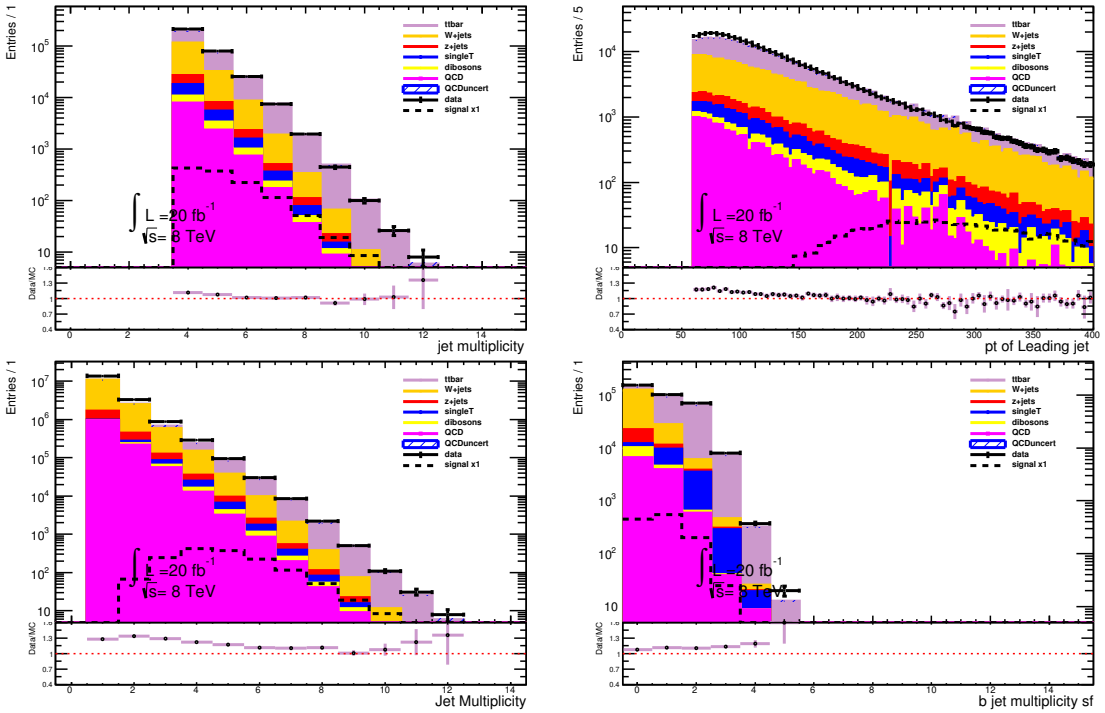

Figure A.1. Plots are obtained in muon channel, top left plot shows jet multiplicities after Cut 20 and applied W+jet reweighting, bottom left plot shows the same distribution before the W+jet reweighting and Cut 20. Top right plot refers the leading jet P_T distribution after loose analysis and bottom right plot shows b-jet weighted jet multiplicities.

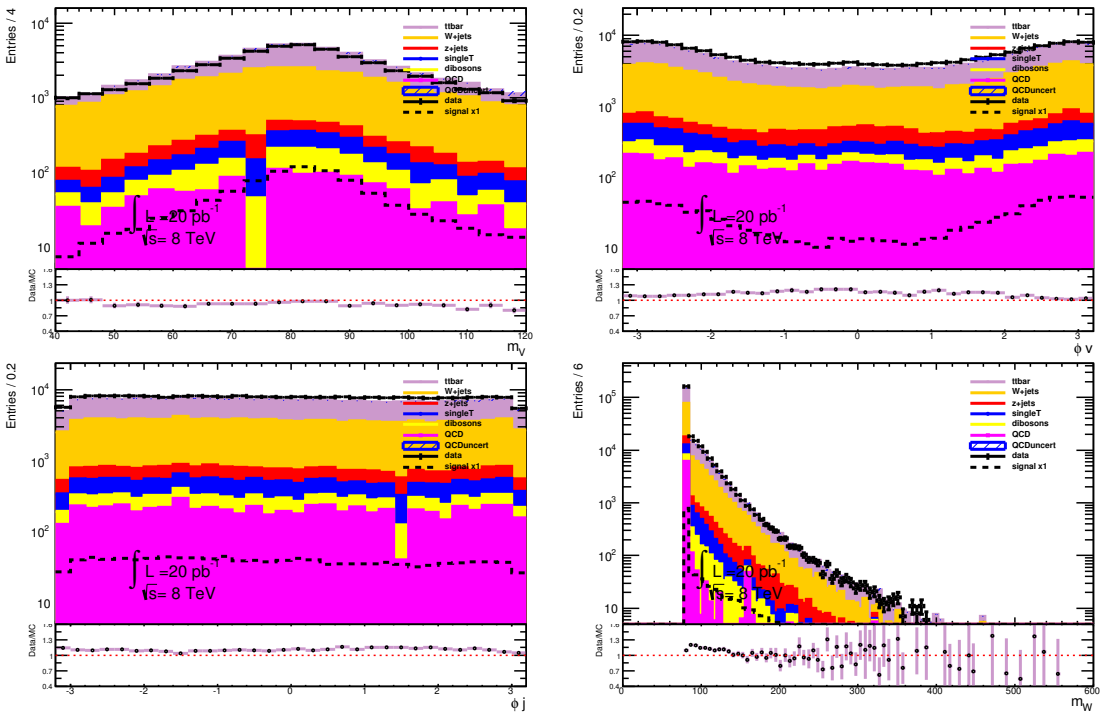

Figure A.2. Plots are obtained in muon channel, reconstructed hadronic W mass, $\Delta\phi$ between the leading jet and E_T^{miss}, ϕ distributions of the leading jet, reconstructed leptonic W mass.

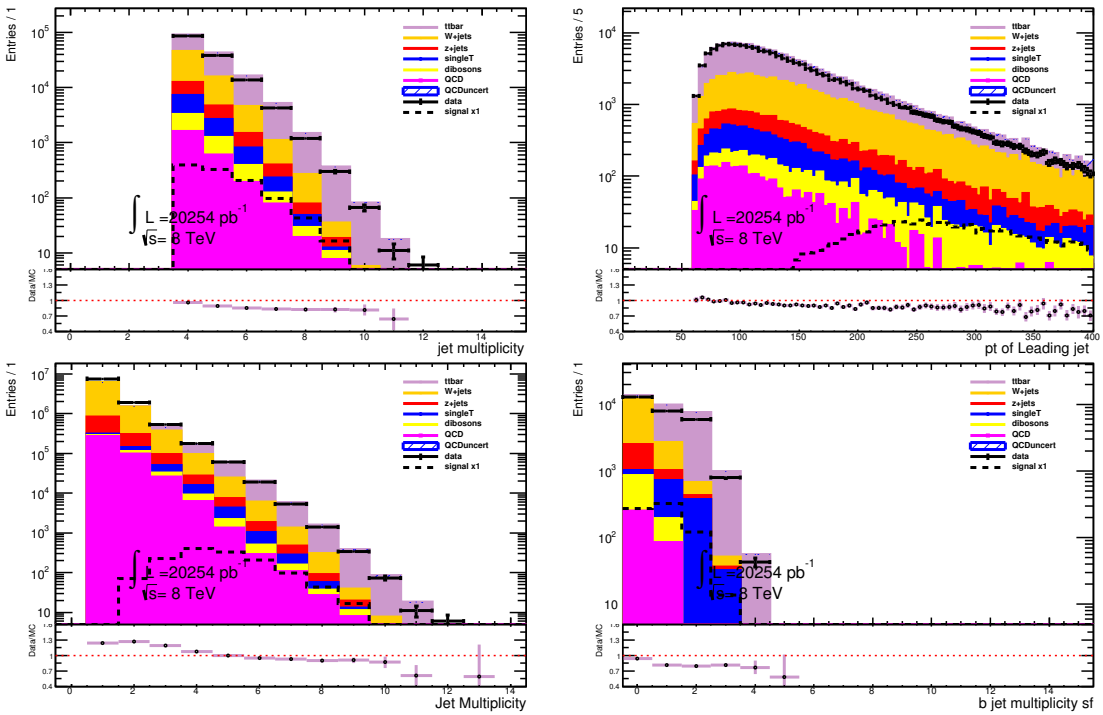

Figure A.3. Plots are obtained in electron channel, top left plot shows jet multiplicities after Cut 20 and applied W+jet reweighting, bottom left plot shows the same distribution before the W+jet reweighting and Cut 20. Top right plot refers the leading jet P_T distribution after loose analysis and bottom right plot shows b-jet weighted jet multiplicities.

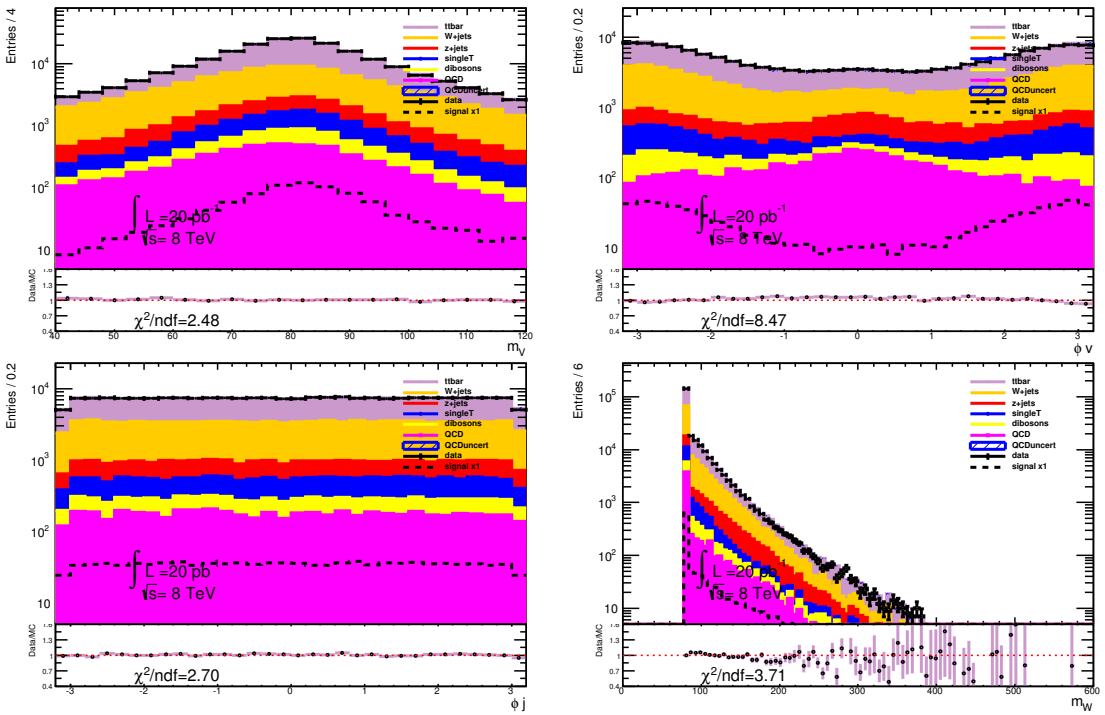

Figure A.4. Plots are obtained in electron channel, reconstructed hadronic W mass, $\Delta\phi$ between the leading jet and E_T^{miss}, ϕ distributions of the leading jet, reconstructed leptonic W mass.

APPENDIX B: CONTROL REGIONS

B.1. Control Region with 3 jets

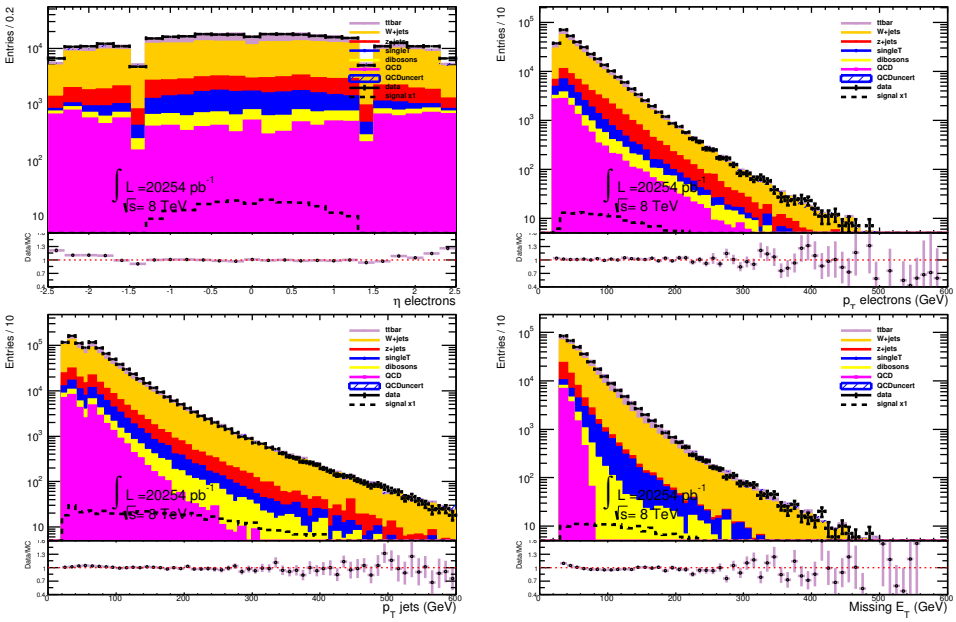

Figure B.1. P_T and η of electrons, P_T of jets, E_T^{miss} distribution in electron channel only with 3 jets.

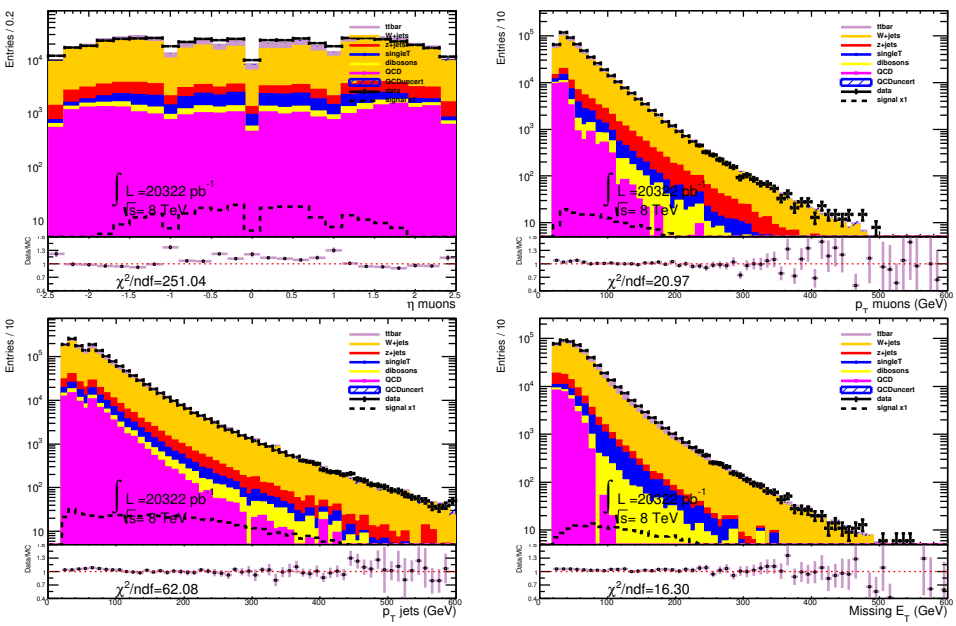

Figure B.2. P_T and η of muons, P_T of jets, E_T^{miss} distribution in muon channel only with 3 jets.

B.2. Control Region with 2 jets

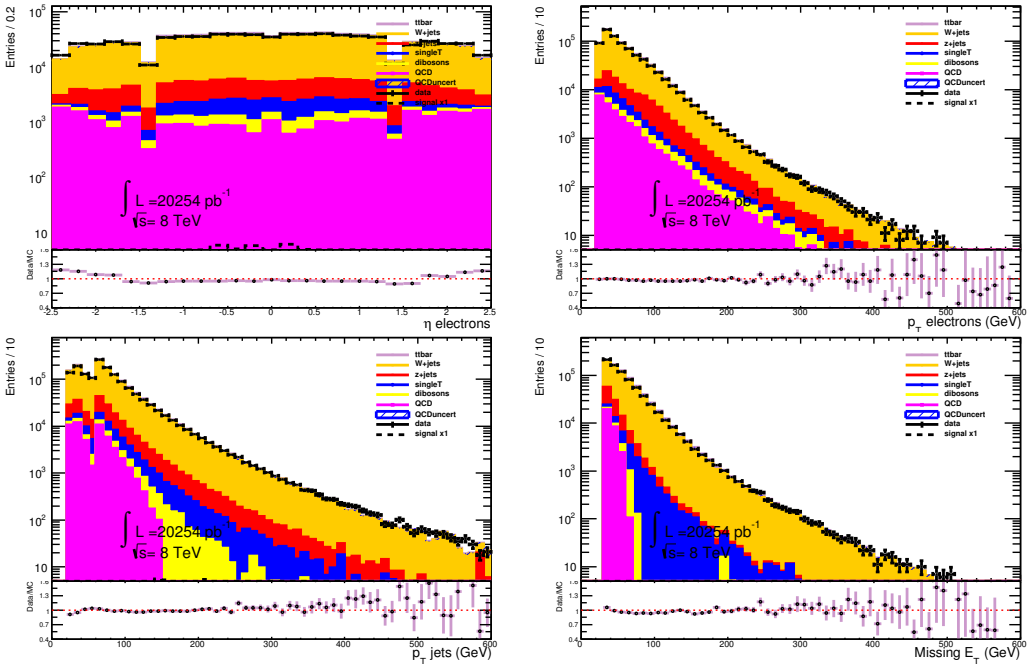

Figure B.3. P_T and η of electrons, P_T of jets, E_T^{miss} distribution in electron channel only with 2 jets.

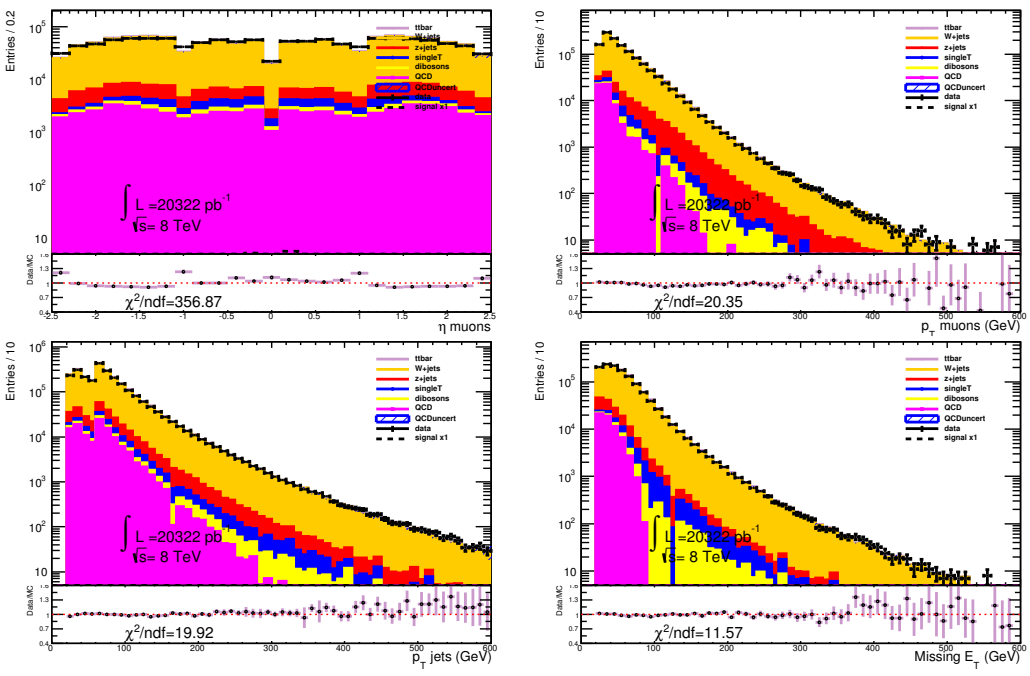

Figure B.4. P_T and η of muons, P_T of jets, E_T^{miss} distribution in muon channel only with 2 jets.

B.3. Control Region only with 1 jet

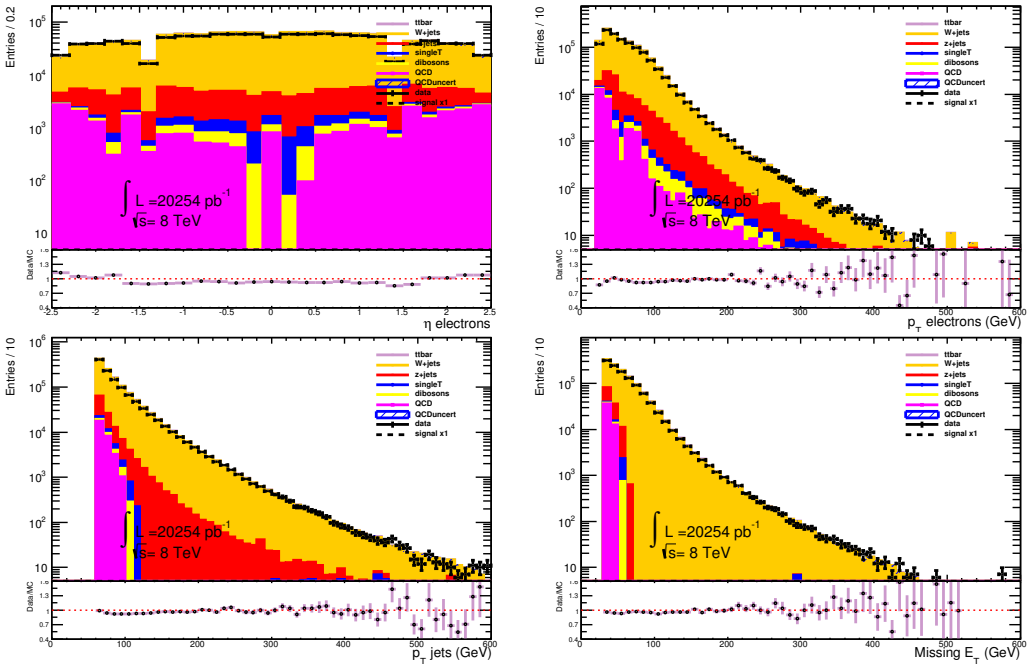

Figure B.5. P_T and η of electrons, P_T of jets, E_T^{miss} distribution in electron channel only with 1 jet.

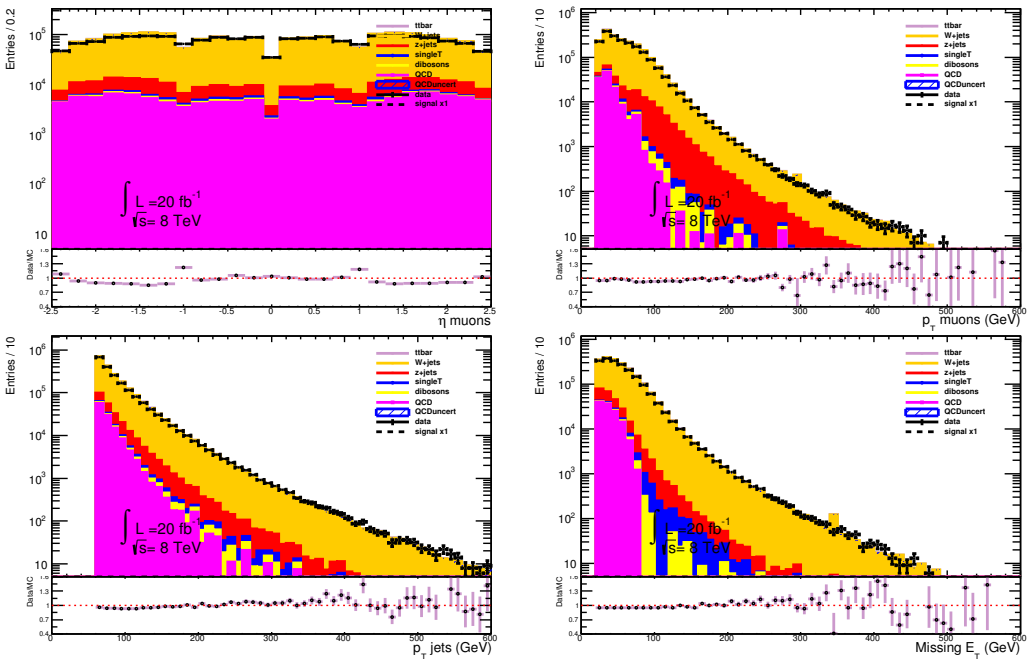

Figure B.6. P_T and η of muons, P_T of jets, E_T^{miss} distribution in muon channel only with 1 jet.

REFERENCES

1. Gagnon, P., "The Standard Model: A Beautiful But Flawed Theory", 2015, http://www.quantumdiaries.org/2014/03/14/the-standard-model-a-beautiful-but-flawed-theory/, [Accessed February 2015].

2. Strassler, M., "The Hierarchy Problem", August 2011, http://profmattstrassler.com/articles-and-posts/particle-physics-basics/the-hierarchy-problem/, [Accessed December 2014].

3. Aliev, M., H. Lacker, U. Langenfeld, S. Moch, P. Uwer, "HATHOR: Hadronic Top and Heavy Quarks Cross Section Calculator", *Computer Physics Communications*, Vol. 182, pp. 1034–1046, 2011.

4. ATLAS Collaboration, JINST 3 (2008) S08003, 2008.

5. ATLAS Collaboration, "Observation Of A New Particle In The Search For The Standard Model Higgs Boson With The ATLAS Detector At The LHC", *Physics Letters B*, Vol. 716, No. arXiv:1207.7214, pp. 1-29, 2012.

6. ATLAS IBL Collaboration, "ATLAS IBL Pixel Upgrade", *Nuclear Physics B*, Vol. 215, No. arXiv:1104.1980 [physics.ins-det], p.147, 2011.

7. ATLAS Collaboration, "Performance Of The ATLAS Trigger System In 2010", *European Physics Journal*, Vol. C72, No. arXiv:1110.1530 [hep-ex], p. 1849, 2012.

8. Kaushik, V. S., "Electromagnetic Showers And Shower Detectors", 2002, http://www-hep.uta.edu/hep_notes/general/general_0001.pdf, [Accessed September 2014].

9. ATLAS Collaboration, "Expected Performance Of The ATLAS Experiment - Detector, Trigger And Physics", arXiv:0901.0512, CERN-OPEN-2008-020, 2008.

10. ATLAS Collaboration, “Expected Electron Performance In The ATLAS Experiment“, Tech. Rep. ATL- PHYS-PUB-2011-006, CERN, Geneva, 2011.

11. ATLAS Collaboration, “Electron Performance Measurements With The ATLAS Detector Using The 2010 LHC Proton-Proton Collision Data”, *European Physics Journal*, Vol. C72, p. 1909, 2011.

12. ATLAS Collaboration, ”Measurement of the Muon Reconstruction Performance of The ATLAS Detector Using 2011 and 2012 LHC Proton–Proton Collision Data“, *European Physics Journal*, Vol. C74, No. arXiv:1407.3935. [hep-ex], CERN-PH-EP-2014-151, p. 3130, 2014.

13. ATLAS Collaboration, “Preliminary Results On The Muon Reconstruction Efficiency, Momentum Resolution And Momentum Scale In ATLAS 2012 pp Collision Data”, Tech. Rep. ATLAS-CONF-2013-088, CERN, Geneva, 2013.

14. GEANT4 Collaboration, S. Agostinelli et al., *Nuclear Instruments and Methods A*, Vol. 506, pp. 250–303, 2003.

15. Mangano, M. L., M. Moretti, F. Piccinini, R. Pittau and A. D. Polosa, “ALPGEN, A Generator For Hard Multiparton Processes In Hadronic Collisions”, *Journal Of High Energy Physics*, Vol. 0307, p. 001, 2003.

16. Corcella, G., I. Knowles, G. Marchesini, S. Moretti, K. Odagiri et al., “HERWIG 6: An Event Generator For Hadron Emission Reactions With Interfering Gluons (Including Supersymmetric Processes)”, *Journal Of High Energy Physics*, Vol. 0101, p. 010, 2001.

17. Sjostrand, T., S. Mrenna and P. Z. Skands, “PYTHIA 6.4 Physics And Manual”, *Journal Of High Energy Physics*, Vol. 0605, p. 026, 2006.

18. Gleisberg, T., S. Hoeche, F. Krauss, M. Schonherr, S. Schumann et al., “Event Generation With SHERPA 1.1”, *Journal Of High Energy Physics*, Vol. 0902, p. 007,

2009.

19. Kersevan, B. P. and E. Richter-Was, "The Monte Carlo Event Generator AcerMC Versions 2.0 To 3.8 With Interfaces To PYTHIA 6.4, HERWIG 6.5 and ARIADNE 4.1", *Computer Physics Communications*, Vol. 184, pp. 919–985, 2013.

20. Frixione, S., P. Nason and C. Oleari, "Matching NLO QCD Computations With Parton Shower Simulations: The POWHEG Method", *Journal Of High Energy Physics*, Vol. 0711, p. 070, 2007.

21. A. Martin, W. Stirling, R. Thorne and G. Watt, "Parton Distributions For The LHC", *European Physics Journal*, Vol C63, No. 450, pp. 189–285, ,2009.

22. Kom, C. H., and W. J. Stirling, "Charge Asymmetry In W + jets Production At The LHC", *European Physics Journal*, Vol. C69, pp. 67-73, 2010.

23. ATLAS Collaboration, "Estimation of Non-prompt And Fake Lepton Backgrounds in Final States With Top Quarks Produced In Proton-Proton Collisions At $\sqrt{s}$ = 8 TeV With The ATLAS Detector", Tech. Rep., ATLAS-CONF-2014-058, CERN, Geneva, 2014.

24. Junk, T., Sensitivity, *Exclusion, And Discovery With Small Signals, Large Backgrounds, And Large Systematic Uncertainties*, Tech. rep., FERMILAB.

25. Junk, T., "Confidence Level Computation For Combining Searches With Small Statistics", *Nuclear Instruments and Methods*, Vol. A434, pp. 435–443, 1999.

26. Cacciari, M., G. P. Salam and G. Soyez, "The Anti-kt Jet Clustering Algorithm", *Journal of High Energy Physics*, Vol. 04, No. arXiv:0802.1189. LPTHE-07-03, p. 063, 2008.

27. Lukas, W.,"Fast Simulation For ATLAS: Atlfast-II and ISF", Tech. rep., ATL-SOFT-PROC-2012-065, ATL-COM-SOFT-2012-137, CERN, Geneva, 2012.

28. ATLAS Collaboration, "Performance Of Missing Transverse Momentum Reconstruction In ATLAS Studied In Proton-Proton Collisions Recorded In 2012 At $\sqrt{s} = 8$", Tech. Rep., ATLAS-CONF-2013-082, CERN, Geneva, 2013.

29. ATLAS Collaboration,"Jet Energy Resolution And Reconstruction Efficiencies From In-situ Techniques With The ATLAS Detector Using Proton-Proton Collisions At A Center Of Mass Energy $\sqrt{s} = 7$ TeV", ATLAS-CONF-2013-082, CERN, Geneva, 2013.